Particles II

Access the latest eBook →

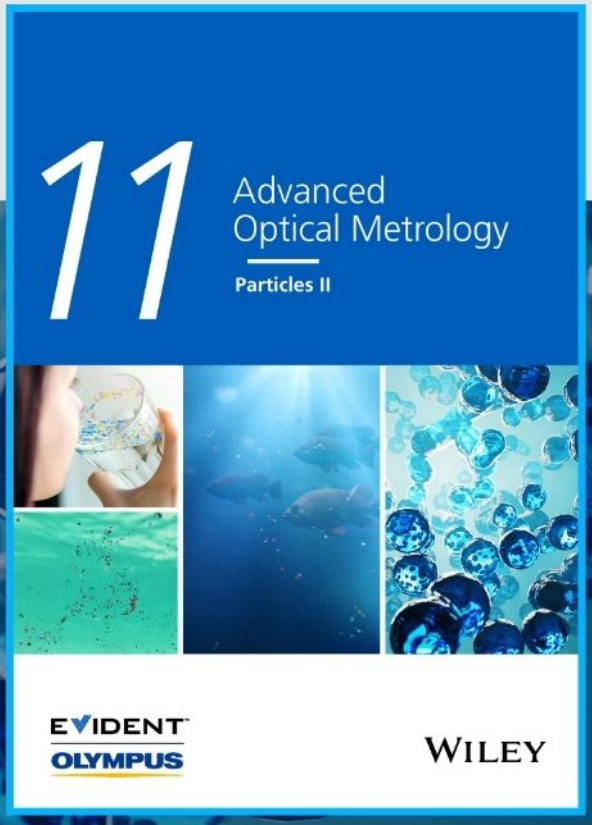

Impact on Biological Systems and the Environment

This eBook is dedicated to the research of Professor David Wertheim.
In collaboration with various groups, Professor Wertheim uses confocal microscopy to analyse the impact of different types of particles on human health and the environment, with a focus on human health-hazardous particles detected with solid-state nuclear track detectors (SSNTD). Download for free, today.

EVIDENT
OLYMPUS

WILEY

ADVANCED MATERIALS INTERFACES
www.advmatinterfaces.de

Self-Healing Superhydrophobic Surfaces: Healing Principles and Applications

*Siyuan Xiang and Wendong Liu**

Superhydrophobic surfaces have already been applied in anti-fouling, water-oil separation, liquid transportation, etc. Surfaces can be defined as superhydrophobic surfaces once they can support a water droplet with its spherical shape maintained and accompanied by an apparent contact angle larger than 150° and a rolling-off angle below 10°. Such water repellent property is achieved by the synergetic action of hierarchical structures and the low-surface energy of the substances constructing the surface. Structures with high aspect ratio always perform good superhydrophobicity. However, they are usually with poor mechanical stability. Since durability is one of the essential factors for practical use, exploiting robust superhydrophobic surfaces has attracted tremendous interest. During the past decade, great effort has been made in developing self-healing superhydrophobic surfaces to improve the potential practice and broaden the application fields. An overview of the recent development of self-healing superhydrophobic surfaces is provided in this review. The focus here is particularly on the fabrication process based on specific healing mechanisms and possible applications. Finally, an outlook on future fabrication techniques for durable superhydrophobic surfaces is presented.

1. Introduction

Superhydrophobic surfaces display extreme water repellency with an apparent contact angle (CA) of water above 150°, meanwhile, the rolling-off angle below 10°.[1] The water repellency is ascribed to the synergistic action of hierarchical physical structures in nano- or/and microscale and low-surface energy substances. Such action allows an air layer to form in between when depositing the droplet onto the solid surface, making droplet set up Cassie–Baxter contact, maintaining its spherical shape, and preventing the liquid from wetting the hierarchical structures.[2] Therefore, the ability to maintain or regain the Cassie–Baxter contact is the crucial factor when considering superhydrophobicity durability. Due to low adhesion and the small contact area between the liquid droplet and solid surface, superhydrophobic surfaces are regarded as promising candidates in anti-corrosion,[3] self-cleaning,[4] anti-fouling,[5] oil/water separation,[6] and others.[7] However, practical uses are greatly limited due to the poor stability.[8] Therefore, conquering the barrier of superhydrophobicity durability has been of great significance.

The water repellency of a superhydrophobic surface can be dramatically damaged in two ways: 1) physical structure loss induced by impact or abrasion, which resulted in the increase of contact area between a liquid droplet and solid substrate; 2) low-surface energy degradation caused by contamination, irradiation, or the damage of the hydrophobic layer.[9] Various approaches have been proposed to enhance the durability, for example, introducing more rigid materials to prepare hierarchical physical structures against mechanical abrasion, employing inert hydrophobic substances to slow down the degradation of intrinsic hydrophobicity, and developing bulk superhydrophobic surface (without hierarchical structures) to extend the durability.[10] Even though superhydrophobic surfaces' lifetime improved through these approaches, the limited extension of durability still confines the consideration of potential applications.

Different from artificial structures, plant leaves, bird feathers, or insect wings can efficiently maintain their liquid repellency by continuously generating the epicuticle wax layer or natural renewal of the micro- or nanostructure after being destroyed.[9,11] Inspired by the self-healing behavior of natural plants and animals, researchers have developed various self-healing superhydrophobic surfaces so as to improve durability and prolong the lifetime for outdoor applications. In this case, an additional supply of low-surface energy substances is not needed.[1b,12] The principle of durability enhancement relies on the preservation of low-surface energy substances inside the hierarchical structures or/and restoration of physical structures. When the liquid repellency gets damaged, the stored low-surface energy substances can be transferred to the top layer of the structure and minimize the surface energy, resulting in the healing of intrinsic hydrophobicity. On the other hand,

Dr. S. Xiang, Dr. W. Liu
Max Planck Institute for Polymer Research
Ackermannweg 10, D-55128 Mainz, Germany
E-mail: liuwendong@mpip-mainz.mpg.de
Dr. W. Liu
School of Chemical Engineering
Dalian University of Technology
Linggong Road 2, Dalian 116024, P. R. China
The ORCID identification number(s) for the author(s) of this article can be found under https://doi.org/10.1002/admi.202100247.

DOI: 10.1002/admi.202100247

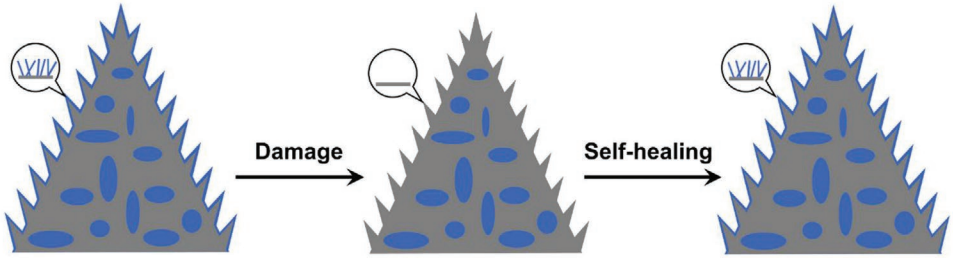

Figure 1. Principle of self-healing superhydrophobic surfaces based on the transportation of low-surface energy substances. Blue represents the low-surface energy substances, and gray represents the basic physical structure.

the regeneration of physical structures can restore the surface topography after the roughness damage.

In this review, we first provide an overview of preparing self-healing superhydrophobic surfaces according to different healing principles. Then we introduce some typical applications of superhydrophobic surfaces with enhanced durability. Finally, we give an outlook on developing the fabrication techniques for durable superhydrophobic surfaces, which could take place in future research.

2. Self-Healing Superhydrophobic Surfaces Based on Specific Healing Principles

The essential advantage of self-healing superhydrophobic surfaces is to enhance the durability of the surface in the process of practical uses. With a self-healing process, surface can recover its liquid repellency after being damaged without extra addition or modification of low-surface energy substances. For superhydrophobic surfaces, superhydrophobicity depends on the coordination of low-surface energy materials and topological physical structures. Therefore, the self-healing process mainly relies on low-surface energy rebirth and the regeneration of topological structures. Self-healing superhydrophobic surfaces can be assorted into three categories based on the following healing processes: transportation of low-surface energy substances to the surface; regeneration of hierarchical topography; the coordination of both. According to the damage or degradation mechanism/condition of the surface, one of these three approaches is required.

2.1. Transportation of Low-Surface Energy Substances to the Surface

Transportation of low-surface energy substances to the surface is the most commonly used approach to regain liquid repellency when they were chemically degraded. Supernumerary low-surface energy substances are persevered in hierarchical structures to mimic the self-restoration of the hydrophobic epicuticle wax layer carried out in natural plant leaves. As shown in **Figure 1**, when the low-surface energy layer is decomposed or degraded, the preserved low-surface energy substances in the structures are then released automatically or under external stimuli treatment (e.g., humidity, UV light, temperature, etc.). The released hydrophobic substances transport to the degraded region and heal the surface chemistry, resulting in the self-healing of the superhydrophobicity. Here, the directed transportation is automatically triggered, driven by the difference of surface energy between the damaged region (high-surface energy) and the released substances (low-surface energy).

Wang et al. developed a self-healing superhydrophobic poly(dimethylsiloxane) (PDMS)/*n*-nonadecane wax composite surface by means of a two-step replication approach to mimic the structure on Lotus leaf.[13] The replicated papilla structure provided the surface with desirable roughness, while the *n*-nonadecane wax supplied the low-surface energy. The amount of preserved *n*-nonadecane wax is about 10 wt% in the physical structure. The coordination of these two factors can reserve air pockets between the wax-coated physical structures endowing the surface with superhydrophobicity. Water droplets (15 µL) deposited on the surface showed an apparent CA of 158°, while a sliding angle (SA) of 9°. The self-healing property of the surface was demonstrated by O_2 plasma treatment to increase the surface energy. After 6 min O_2 plasma etching, the wax layer was etched off and enriched with hydroxyl groups, resulting in superhydrophilicity of the surface whose water CA of 0° (**Figure 2**a). Interestingly, after stored at room temperature for 20 min, the surface regained its water repellency with a water CA of about 160°. The self-healing behavior is repeatable (Figure 2b,c). After cycles of plasma damaging and automatically self-healing processes, the surface still maintained its superhydrophobicity with large CA (above 150°) and small SA (around 11° for 15 µL drop). The basic process of such self-healing behavior is shown in Figure 2d, which is attributed to the preserved wax's transportation in the physical structures. After plasma treatment, the low-surface energy material, *n*-nonadecane wax, was etched off, and the surface became hydrophilic with high-surface energy. The interface free energy between the hydrophilic surface and air is larger than that between hydrophobic wax and air. Thus, such differences in interface free energy drive the transportation of hydrophobic wax from the PDMS matrix to the surface, reducing the surface energy meanwhile recovering the rough fibers on the microscale structures. The ability of wax to migrate from bulk PDMS structures is attributed to the relatively low melting point of *n*-nonadecane, 32 °C, which endowed the wax molecules with a fast migration speed at room temperature (25 °C). Moreover, the high mobility of PDMS molecular chains provided additional freedom for the diffusion of *n*-nonadecane molecules in the PDMS network. The synergism of these two factors leads to fast transportation dynamics of hydrophobic wax molecules from the physical structures to the outer surface to heal the superhydrophobicity. It is worth noting that the low melting

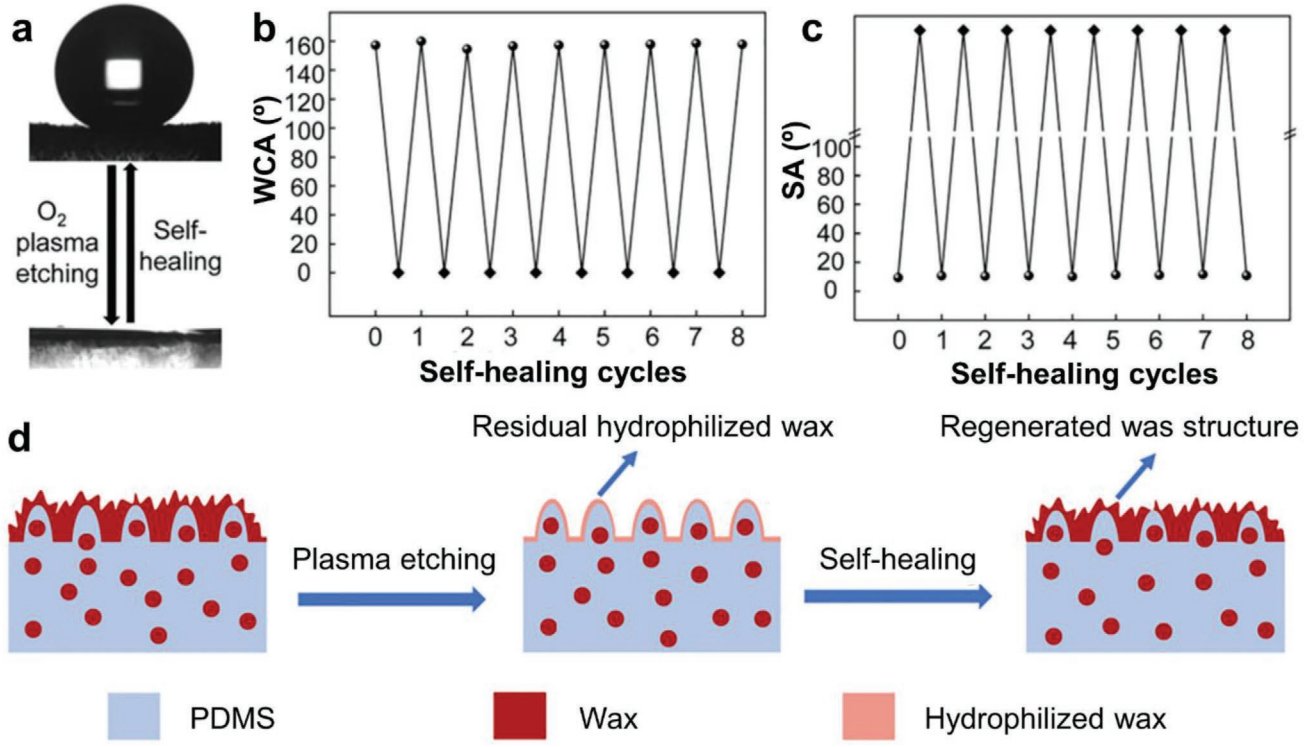

Figure 2. a) Reversible transition between superhydrophobic and superhydrophilic states of PDMS/*n*-nonadecane upon O_2 plasma etching and self-healing. b) Change of water CA and c) SA (15 µL droplet) of PDMS/*n*-nonadecane in repeated etching–healing tests. The rhombuses indicate data on the etched surface and the circles indicate data on the self-healed surface. No physically meaningful SA is available for plasma-etched surface as a water droplet will spread on the surface. d) Schematic showing the self-healing mechanism of the prepared biomimetic superhydrophobic surface. a–d) Reproduced with permission.[13] Copyright 2020, Elsevier.

point of wax ensured that such fast self-healing behavior could be conducted at room temperature, avoiding additional energy consumption caused by external stimuli.

By spray coating, a substrate with polyelectrolyte complexes of poly (allylamine hydrochloride)-sulfonated poly (ether ether ketone) (PAH-SPEEK), poly (acrylic acid) (PAA), and healing agent of perfluorooctanesulfonic acid lithium salt (PFOS), Li et al. also developed self-healing superhydrophobic surfaces.[14] Porous and rough (PAA/PAH-SPEEK)*n structures formed after alternatively spraying PAA and PAH-SPEEK. After coating additional PFOS on the (PAA/PAH-SPEEK)*80 structure, the surface energy was further decreased, and the superhydrophobic surface of PFOS-(PAA/PAH-SPEEK)*80 achieved. Taking advantage of the electrostatic interaction between the sulfonate group and the protonated amine groups of the PAH, PFOS was persevered in the (PAA/PAH-SPEEK)*80 structure and served as a healing agent through a spraying process. The self-healing performance was also evaluated by O_2 plasma etching to mimic the degradation of surface chemistry. As shown in **Figure 3**a, the surface changed from superhydrophobic into superhydrophilic with a water CA of 0° after O_2 plasma etching for 1 min, demonstrating that the PFOS layer was decomposed and hydrophilic groups formed on the (PAA/PAH-SPEEK)*80 surface. The enhanced surface energy together with rough structures endowed the etched surface with superhydrophilicity. However, after exposing the damaged surface under an ambient environment with a relative humidity (RH) of 40% for 4 h, the superhydrophobicity was recovered. The preserved PFOS in the rough structures get released and transported to the surface to re-decrease the surface energy. Meanwhile, the polar hydrophilic groups originated by O_2 plasma treatment were embedded inside the polyelectrolyte coating. In this way, superhydrophobicity was self-healed. Owing to the electrostatic interaction between PAA and PAH-SPEEK layers, the as-prepared PFOS-(PAA/PAH-SPEEK)*80 surface displays satisfactory mechanical stability to ensure long-term self-healing behavior. The PFOS-(PAA/PAH-SPEEK)*80 surface was able to retain its superhydrophobicity after repeating the etching–healing processes for several rounds with only an insignificant change of water CA could be observed while small SA maintained (Figure 3b,c). Utilizing the full spray coating method, a superhydrophobic surface can be prepared 25 times faster than the conventional layer-by-layer assembly approach. Moreover, the superhydrophobic coating can regain its self-healing property by re-spraying low-surface energy substance POTS (1H,1H,2H,2H-perfluorooctyltriethoxysilane) once after the preserved healing agents consumed by multiple healing processes (Figure 3c).

In another approach, self-healing superhydrophobic surfaces were obtained by loading the low-surface energy substances in porous structures or in capsules constructed in the superhydrophobic layer.[15]

Chen et al. prepared a waterborne self-healing multiple protective superhydrophobic fabric coating.[16] Core-shell cellulose-silica/*n*-octadecane microcapsules were first synthesized

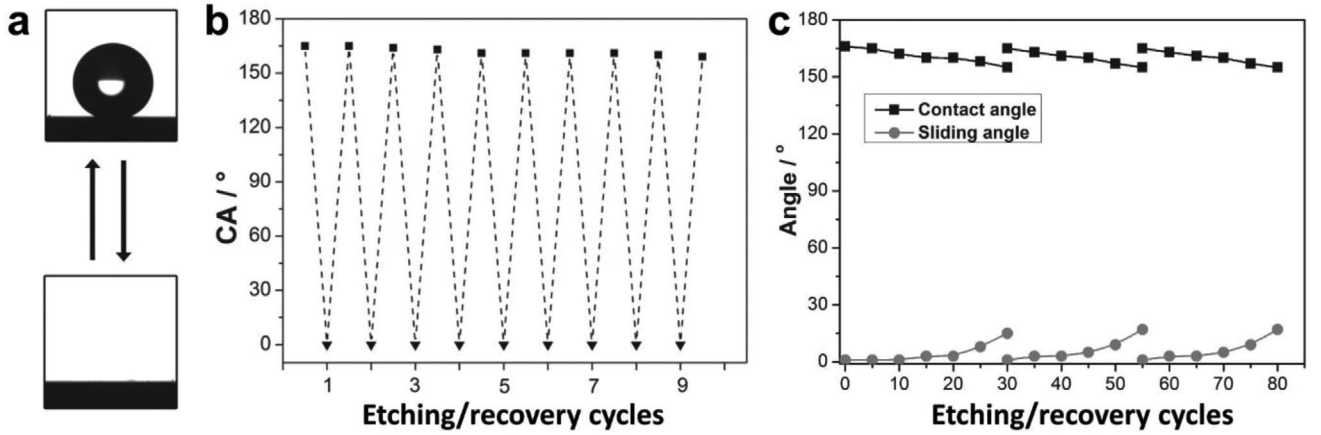

Figure 3. a) CA of PFOS-(PAA/PAH-SPEEK)*80 coating after O_2 plasma etching (bottom) and self-healing (top). b) Change in the CA of the O_2 plasma-treated PFOS-(PAA/PAH-SPEEK)*80 coating (▲) and self-healed coating (■). c) Changes in the CA (■) and SA (●) of the POTS/PFOS-(PAA/PAH-SPEEK)*80 coatings after O_2 plasma etching–healing cycles. The POTS solution is re-sprayed on the 30th and 55th cycles. a–c) Reproduced with permission.[14] Copyright 2014, Wiley-VCH.

using a one-step emulsion-solvent diffusion method, during which hydrophobic coupling reagent (perfluorooctyltriethoxysilane (FAS-13), 3-isocyanatopropyltriethoxysilane) and UV absorber (Tinuvin 400) persevered in the silica shell. Then the microcapsules were dispersed into waterborne silicone resins and used for the preparation of coating on fabrics. Attributed to the micrometer size of capsules and the hydrophobic molecules grafted on the shell, the coated fabric presented superhydrophobicity with a water static CA of about 155° while rolling-off angle of about 7° (**Figure 4**a). Besides pure water, the as-prepared coating could also show repellency to some other liquids (e.g., orange juice, milk, soy sauce, tea, coffee, and saturated salt water) in daily uses. Such kind of surface possessed outstanding durability. The coating maintained its superhydrophobicity even after treated with acidic/basic liquids, heated under different temperatures (from 0 to 120 °C), and washed 10 times with the standard washing process. Moreover, due to the UV blocking agents grafted on the silica shell, the superhydrophobic coating could absorb UV light at 250–350 nm. After 168 h of an accelerated aging test, the surface still maintained superhydrophobic, which performed superior UV protection property, making it more promising for practical applications, especially for those under solar radiation. The composite coating also showed self-healing property, which was evaluated by damaging the top layer's hydrophobic substances either by chemical immersing or mechanical abrading. After treated with a surface-active solution (Triton X-100, 3 wt%) for 30 min, the surface became hydrophilic with a CA of about 65° due to hydrophilic groups' formation on the surface (Figure 4a). However, after heating the fabric at 80 °C for 15 min, the surface repellency recovered. In addition, when the surface was mechanically damaged by sandpaper under 10 kPa pressure, the surface's water repellency was reduced to a hydrophobic state with a CA of about 135°. Again, the liquid repellency recovered to superhydrophobic state after heating the fabric at 80 °C for 30 min (Figure 4b). In both cases, the superhydrophobicity can be healed by heating at 80 °C for a certain time after several rounds of liquid repellency degradation. The self-healing property was mediated by the transportation of hydrophobic components preserved in the microcapsules, as illustrated in Figure 4c. The destruction of the hydrophobic substances on the surface, either by chemical or mechanical manner, results in the degradation of its water repellency. The physical structure was maintained even after mechanical abrasion since the microcapsules embedded in the coating will be exposed to retain the topography. Thus, the recovery of hydrophobicity on the surface became the critical point. In their work, hydrophobic components were already preserved in the microcapsules during the synthesis step and exhibited high flexibility due to their long-chain conformation. Once the damaged coating was heated, the hydrophobic components will be migrated to the surface to minimize the surface free energy, resulting in the healing of superhydrophobicity. Thus, the surface could still maintain its superhydrophobicity after many damage-healing processes, which endowed the coating with prolonged durability to meet specific practical requirements.

Similarly, Chen et al. achieved a self-healing superhydrophobic surface by using UV-responsive microcapsules as building blocks.[17] Using TiO_2 and SiO_2 nanoparticles as the Pickering agents, low-surface energy substance (dodecafluoroheptylpropyl-trimetoxysilane, FAS-12) loaded UV-responsive microcapsules were synthesized via Pickering emulsion polymerization of styrene. The prepared microcapsules were mixed with heptadecafluoro-1,1,2,2-tetradecyl trimethoxysilane (FAS-17)-modified SiO_2, and polysiloxane latex, and then coated on a target substrate to obtain superhydrophobic surface. Once the surface was mechanically damaged or contaminated by oil, its liquid repellency can be self-healed after experiencing UV irradiation. When being exposed under UV irradiation, the preserved FAS-12 in the microcapsules was released as a result of the photo-catalyzed degradation of polystyrene. The released FAS-12 then migrated to the damaged area to comprise the surface energy difference, resulted in the recovery of superhydrophobicity. The obtained superhydrophobic surface can maintain its liquid repellency in an outdoor environment for more than 2160 h. Meanwhile, the damaging-healing process can be repeated for at least ten cycles without a loss of liquid repellency, indicating its finely improved durability for outdoor applications.

All the self-healing superhydrophobic surfaces mentioned above relied on fluorine-compounds. However, fluorine materials

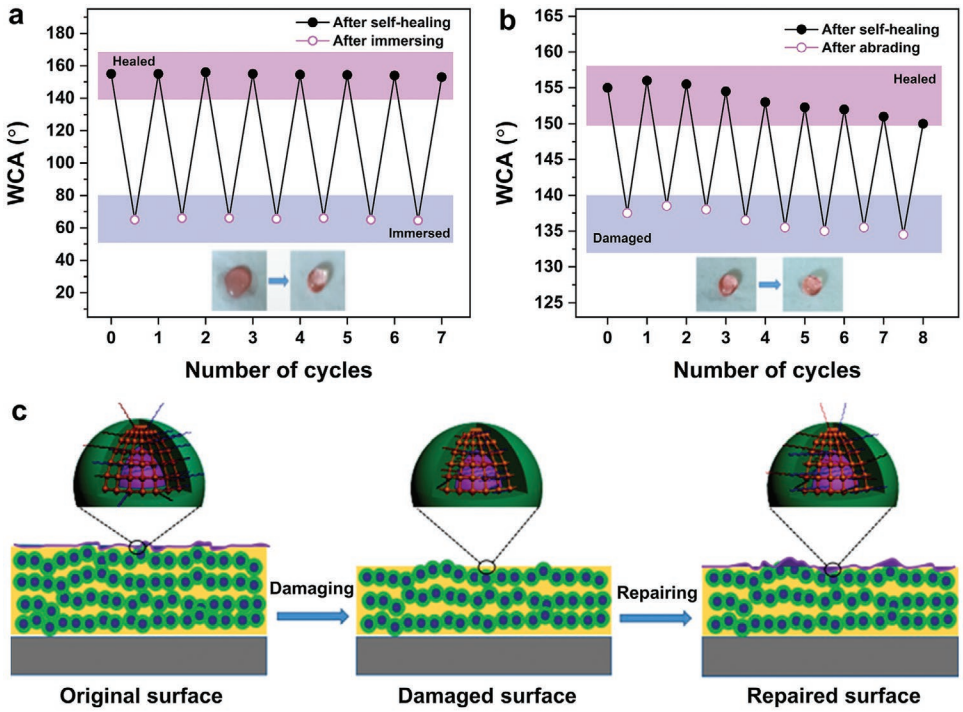

Figure 4. Variations of water CA with the repeated process of either surfactant immersing (a) or abrading (b) and repairing. c) The self-healing mechanism diagram of multiple protective fabric coatings. a–c) Reproduced with permission.[16] Copyright 2020, Elsevier.

can be easily decomposed and released into the environment, which is unfavorable to humans and wildlife. Thus, considerable efforts have been made to prepare self-healing superhydrophobic surfaces with a self-healing process based on fluorine-free substances.[18] Such fluorine-free and environmentally friendly surfaces are more beneficial and suitable for practical use, which can further broaden the application fields of superhydrophobic surfaces.

By depositing H_3BO_3-incorporated SiO_2-alkyl-silane on cotton followed by PDMS modification, Lahiri et al. were able to prepare a robust fluorine-free and self-healing superhydrophobic coating.[19] The coated surface demonstrated excellent water repellency, with a 5 µL water droplet deposited on it presented a large CA of 158° and a small sliding hysteresis angle of 4°. Modification of PDMS endowed the surface improved durability and self-healing property. On the one hand, the PDMS acted as an adhesive which glued the micro and nanoscale structures together and enhanced the adhesion with the substrate, contributing to improving the robustness and durability of the coating. The coated fabric still maintained its superhydrophobicity after the reduplicative tape-peeling test (about 80 repetitions, under 48.05 kPa), and sandpaper (Cw-2000) rubbing (loaded 100 g, for 40 cycles). On the other hand, the PDMS acted as a healing agent to recover the damaged superhydrophobicity. Once the surface's water repellency was damaged by air-plasma treatment for 3 min, the embedded PDMS chains can transport to the hydrophilic region, minimizing the surface energy and healing the superhydrophobicity due to their high flexibility and low-surface energy. The self-healing can be automatically triggered and accomplished in 12 h at room temperature. The damaging–healing process can be repeated many times without significant wettability changes, indicating the prolonged durability of the surface and making it suitable for long-term practical uses.

Recently, Zhang et al. also achieved self-healing superhydrophobic surface without using fluorine-substances.[20] All-water-based polydopamine (PDA) coated octadecylamine (ODA) nanospheres were first prepared with large ODA nanospheres as core while thin PDA coating as a shell. These core-shell spheres were further coated onto fabrics by a simple dip-coating process and dried at room temperature. After that, the coated fabric was heated under one sun (1 kW m^{-2}) for 15 min to achieve superhydrophobicity. Benefit from intrinsic adhesion of PDA on many kinds of substrates,[21] the PDA shell can fix the core-shell nanospheres on the fabrics to form hierarchical structures, supplying sufficient surface roughness for superhydrophobicity. With sun light irradiation, the core-shell nanospheres were heated up due to favorable photothermal property of the PDA shell, making the ODA molecules near the shell be easily transported to the surface to provide low-surface energy. Such coordination of hierarchical structure and low-surface energy endowed the coated fabric with superhydrophobicity (**Figure 5**a). Water droplet demonstrated an apparent CA of 161° with a rolling-off angle of about 5°. In addition, for complex aqueous droplets, for example, milk, coffee, and cola, it can also keep a spherical shape, indicating the surface's outstanding superhydrophobicity. After treated with O_2 plasma, the surface wettability was transformed from superhydrophobic to superhydrophilic with a water CA of 0°. However, the damaged superhydrophobicity can be easily recovered after irradiating the surface with one sun for 15 min. The water CA increased to 160° again, while the rolling-off angle maintained below 10°.

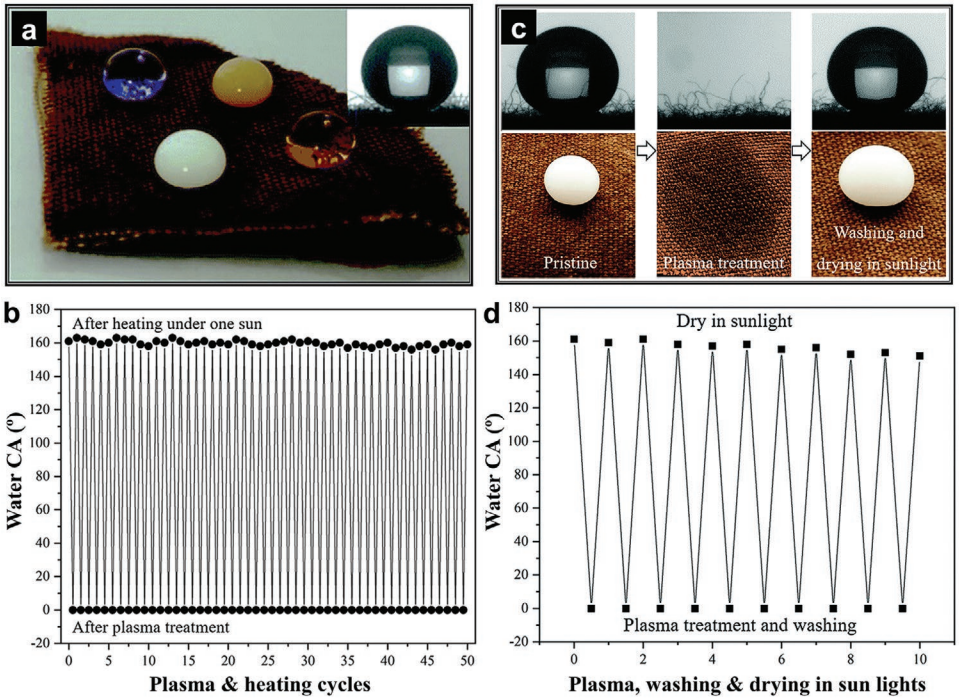

Figure 5. a) Image of various liquids such as water (dyed blue), coffee, milk, and Coca Cola on the superhydrophobic fabric-(ODA@PDA). The inset is the water CA of the fabric. b) CAs of water on the fabric-(ODA@PDA) in the 50 cycles of plasma and heat treatment. c) Photos of milk droplet on the pristine fabric-(ODA@PDA) (left), the fabric after plasma treatment (middle), and the fabric after washing and drying in sunlight (right). d) The change of the water CAs of the fabric-(ODA@PDA) after plasma treatment, washing, and drying in sunlight (under one sun). a–d) Reproduced with permission.[20] Copyright 2019, Royal Society of Chemistry.

The healing process is conducted by the transportation of ODA to the surface, the same as the generation process of superhydrophobicity. O_2 plasma treatment etched the ODA molecules on the surface, resulting in the transformation of superhydrophilicity. Once irradiated with sun light, the PDA shell heated up the nanospheres near the melting point of ODA, accelerating the movement of preserved ODA to the degraded surface, reducing the surface energy, and healing the damaged superhydrophobicity. Due to the high loading amount of low-surface energy substances (ODA) in the core-shell nanospheres, the surface showed outstanding self-healing behavior. Its superhydrophobicity can still be recovered even after 50 cycles of plasma damaging-healing processes (Figure 5b). Moreover, the prepared fabric is also mechanically stable. As shown in Figure 5c, the milk droplet performed a spherical shape on the superhydrophobic surface. Once the surface was damaged by plasma, milk droplet can easily wet the substrate. After washed by a laundering machine for 50 min to remove the milk stains and dried under sunlight, the superhydrophobicity recovered again with the CA of milk droplet back to about 159°. The micro-nano structures remained on the fabrics even after ten times washing and drying under sunlight, accompanied by the recovering of superhydrophobicity (Figure 5d), indicating that the coating possesses outstanding durability against mechanical damage, which makes it great potential in water-proof clothes.

Similarly, Liu et al. achieved a fluorine-free self-healing superhydrophobic surface by spraying an all-in-one suspension of aluminum phosphate, TiO_2 nanoparticles, and octadecyltrichlorosilane (OTS) on a substrate.[22] Herein, OTS acts as surface modification and healing substance, providing low-surface energy for the rough structure and restored liquid repellency after damage. When the surface was decomposed by hot water, O_2 plasma, and amphiphiles, the superhydrophobicity healed after experiencing a high temperature treatment. The healing property is attributed to the release of embedded OTS and migration to the damaged area. In addition, another type of fluorine-free, self-healing superhydrophobic surface was prepared by Zeng et al. through in situ growing zirconium phosphate (ZrP) nanoplates on textiles and followed by filtration of low-surface energy healing agent, ODA.[23] After experiencing a plasma etching process, the degraded superhydrophobicity was healed by exposing the surface to air for 48 h at room temperature. The liquid repellency could be resorted in a short time by heating the degraded surface to 65 °C to accelerate the thermal transportation of ODA to the damaged area and minimize the surface energy.

These fluorine-free approaches have broadened the fields that self-healing superhydrophobic surfaces can be used, for example, cleanup of oil spills, fuel purification, and water treatment.

It is worth noting that some of the self-healing processes depend on additional stimuli, for example, UV light, humidity, or temperature, to induce the transportation of low-surface energy substances, limiting the practical application. In other cases, the self-healing could also be carried out in ambient conditions but took a long time. Based on this, further efforts should be focused on both accelerating the self-healing process and inducing the self-healing under more practical conditions.

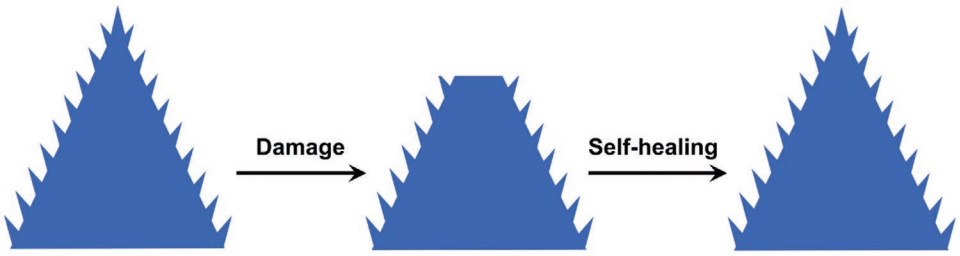

Figure 6. Principle of self-healing superhydrophobic surfaces based on the regeneration of hierarchical topography.

2.2. Regeneration of Hierarchical Topography

Regeneration of surface roughness or topography structure is another approach to heal superhydrophobicity (**Figure 6**). Renewal of topography is usually required after the hierarchical structures being chemically destroyed, for example, abrasion/scratching or crushing. One challenge is to regenerate intrinsic hierarchical structure on different length scales. Researchers have made considerable efforts to prepare superhydrophobic surfaces with self-regenerating topography.[24] In this part, we will provide an overview of how such superhydrophobic surfaces may regenerate their hierarchical topography. Even though the regeneration performance here is not as perfect as natural species that can renew the rough structures by themselves, it is still beneficial to surface wettability recovery and enhanced durability.

One basic approach for surface roughness regeneration is to re-arrange the components in the coating. By the combination of 3-methacryloxypropyltrimethoxysilane (KH570) grafted nano-SiO_2 and aligned carbon nanotube bundles (ACNTB), Wang et al. synthesized ACNTB-SiO_2-KH570 hierarchical particles and further used them to prepare self-healing superhydrophobic surfaces with the coordination of epoxy (EP).[25] The composite surface demonstrated excellent superhydrophobicity with water (4 µL) CA of 160°, while a rolling-off angle of 3°. Here, the particles provided the necessary hierarchical structure and the hydrophobic molecules, KH 570, provided low-surface energy for superhydrophobicity. The surface showed particularly good mechanical stability. After 300 cycles of abrasion with sandpaper (800 grit, loaded with 100 g counterpoise), water droplets on the surface still maintained a CA of 150° with a rolling-off angle of about 8°, indicating the retaining of superhydrophobicity. When the EP/ACNTB-SiO_2-KH570 surface was damaged by sandpaper rubbing and peeled with tape, the surface's water repellency degraded accordingly (water CA decreased to 123°, while rolling-off angle increased to around 40°). However, after heating the damaged surface at 300 °C for 9 h, the surface demonstrated a self-healing behavior. Water CA returns to 160° with a rolling-off angle of about 1°, indicating the recovery of the water repellency (**Figure 7**a,b). SEM characterization showed no apparent nanoparticles but holes caused by particles shedding were observed on the damaged surface, indicating that the deformation of physical structure induced superhydrophobicity degradation (Figure 7c). After the heating treatment, obvious rough nanostructures and nanoparticles were observed again under SEM characterization, showing the physical structure regeneration and the superhydrophobicity recovery (Figure 7d). The water repellency remained after multiple structure damage–regeneration cycles. The schematic self-healing mechanism mediated by structure regeneration is shown in Figure 7e. EP polymers can be partially decomposed during the heating process, leaving the ACNTB-SiO_2-KH570 hierarchical nanoparticles exposed on the surface (Figure 7e(ii,iii)). Besides, the heat can weaken the interaction between CNT and SiO_2. The flow of gaseous products decomposed from EP polymers will further accelerate the transportation and assembly of SiO_2 nanoparticles to reconstruct rough structures on the damaged surface, resulting in the structure regeneration-induced self-healing process.

Similarly, researchers have employed polymers for structure regeneration that relied on rearrangement aggregation. Bai et al. achieved a self-healing superhydrophobic surface by spraying a mixture of zinc stearate (ZNO), polymethylmethacrylate (PMMA), and stearic acid (STA) on to a surface.[26] The ZNO in the mixture formed hierarchical aggregates during the spraying process, endowing the coating with necessary roughness. Meanwhile, the long hydrophobic alkyl chains of STA provide low-surface energy, resulting in water repellency of the obtained surface with water CA up to 158° (**Figure 8**a). After strong droplet impacting, the hierarchical structure deconstructed and the surface became smooth. The super liquid repellency was subsequently lost with water CA reduced to 134° (Figure 8b). The destroyed structure and liquid repellency could be healed by immersing the damaged surface in deionized water for 30 min and then dried at 80 °C (Figure 8c). Superhydrophobicity was recovered after the damage and could be restored repeatedly. The mechanism of hierarchical topography regeneration, in this case, was attributed to the swelling behavior of PMMA in water.[27] As shown in Figure 8d, once the damaged surface is immersed in water which will infiltrate into the damaged structure and trigger the swelling of PMMA. Then the swelled PMMA will regenerate the topographic structures that compressed during the impact. Experienced a drying process, the water in the structure evaporated and left hydrophobic air holes appeared again, followed by the recovery of superhydrophobicity. Such a unique healing process is simple and environmentally friendly, satisfying outdoor application requirements. Recently, Liu et al. achieved a self-healing superhydrophobic surface on a PDMS substrate by replicating the structure of the shark skin, followed by growing poly (2-perfluorooctylethyl methacrylate) (PFMA) via surface-initiated atom transfer radical polymerization (SI-ATRP) (Figure 8e).[28] After soaking the surface in either ethanol or DMF, the PFMA brushes assembled into irregular structures (Figure 8f). Coordination of microscaled groves with

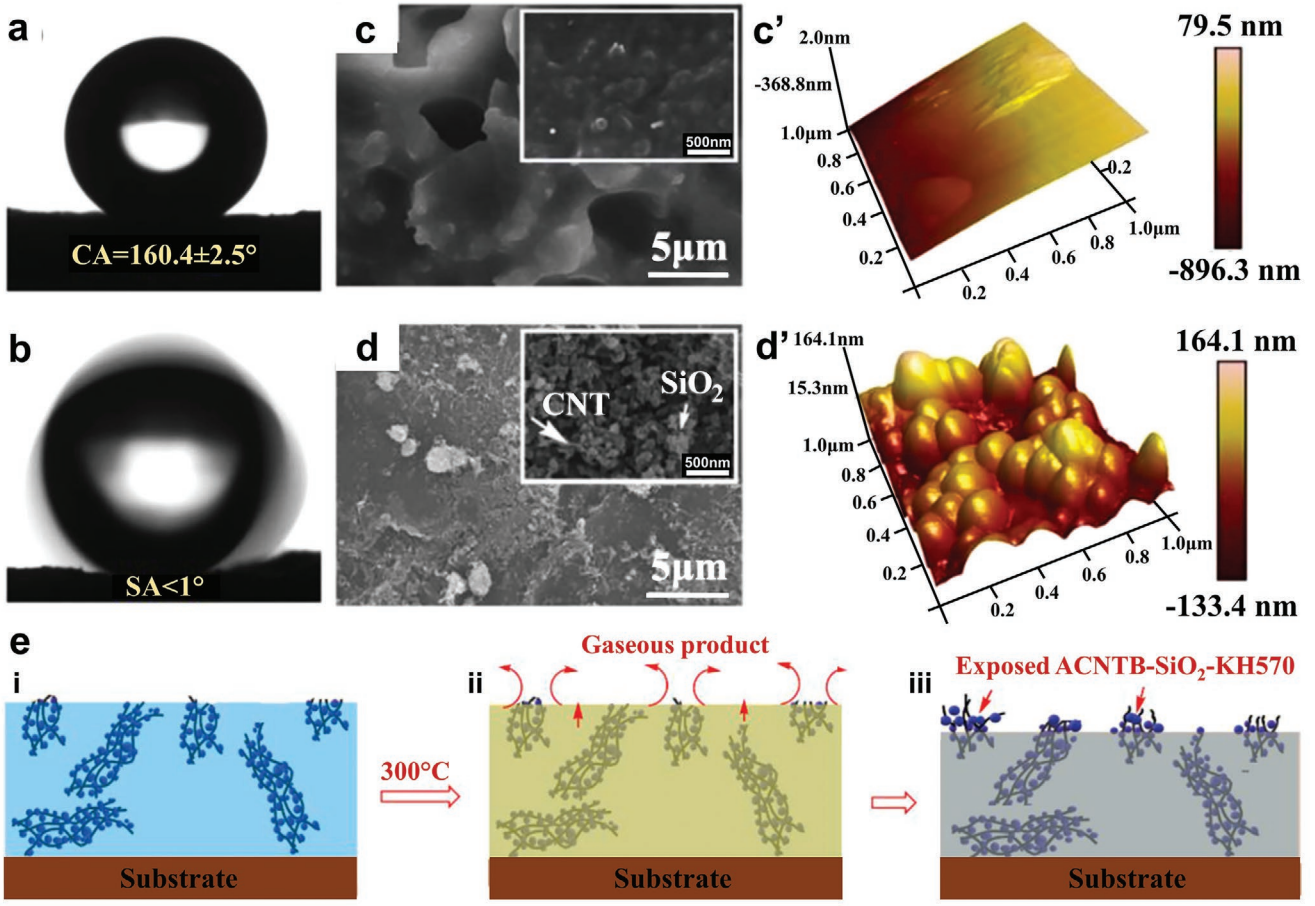

Figure 7. a) CA and b) SA of the damaged EP/ACNTB-SiO2-KH570 coating after heat treatment at 300 °C per 9 h, SEM and AFM images of the damaged coating before (c,c′) and after heat treatment at 300 °C per 9 h (d,d′). e) Schematic of the self-healing mechanism of the superhydrophobicity of the damaged coating. i) The damaged coating without superhydrophobicity, ii) heating the damaged coating at 300 °C per 9 h, iii) the damaged coating after heat treatment at 300 °C. a–e) Reproduced with permission.[25] Copyright 2021, Elsevier.

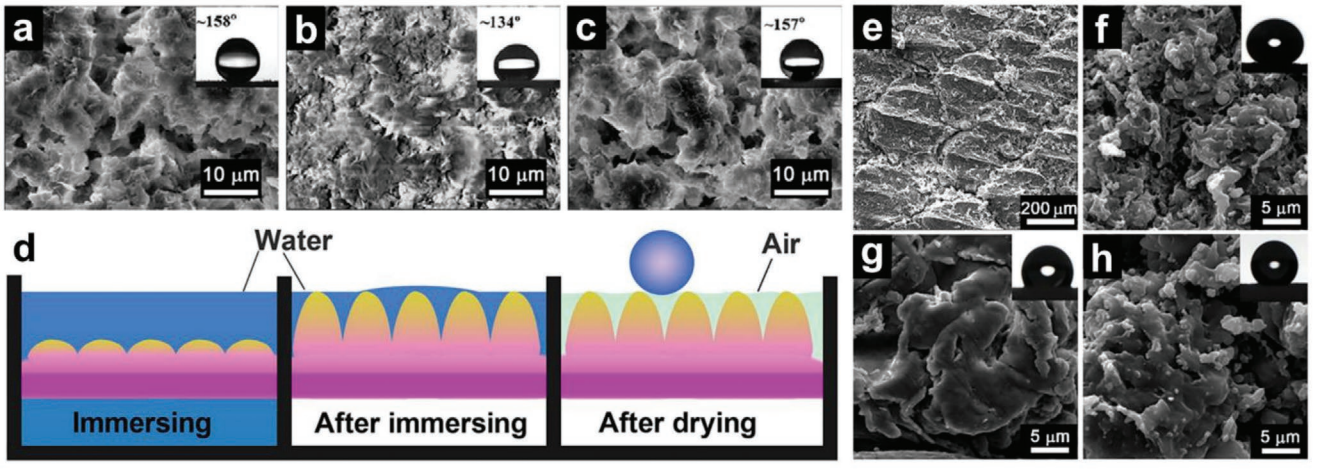

Figure 8. a–c) SEM images of a superhydrophobic coating fabricated from a mixture of PMMA, ZNO, and STA. The superhydrophobic coating before (a) and after (b) damage by droplet impacting, and after recovery of topography by immersion in water and drying at 80 °C (c). The inserts show the CA images corresponding to each morphology. d) Schematic of the self-healing mechanism of superhydrophobic coating. a–d) Reproduced with permission.[26] Copyright 2016, Elsevier. e–h) SEM images of sharkskin-templated PDMS films. e) PDMS film with grooved structure, f–h) topographic structure of enlarged PDMS film: original (f), mechanically damaged (g), and self-recovered (h), insets: water CA photographs of the biomimetic PDMS films in each state. e–h) Reproduced with permission.[28] Copyright 2019, Elsevier.

a size of ≈80 μm and irregular structures of a 0.5–5 μm length scale resulted in the formation of a superhydrophobic surface. CA of 10 μL water droplet was reported to be 158°. With the help of these grove structures, the prepared surface showed wear-resistance. The surface could maintain its water repellency after ten times abrasion with a 1×1 cm^2, 200# sandpaper, loaded with 500 g weight. The samples moved 10 cm over the sandpaper for each abrasion. The hierarchical topography regeneration-based self-healing property was tested by utilizing the finger-wiping test. After the surface was wiped, it became flat with less irregular structure compared to those of the original surface. Such flattening was caused by the aggregation and collapse of PFMA chains as a result of abrasion (Figure 8g). The destroyed structure could be regenerated by treating the damaged surface with DMF for 1 h. Since DMF is a good solvent for PFMA, the polymer brush in the damaged region became mobile and re-assembled into a more irregular structure to recover the surface topography and water repellency (Figure 8h). The damage and self-healing process could be repeated at least eight times, indicating the as-prepared surface was durable enough to be used in practical films.

However, when surfaces are severely scratched and the cuts extended over tens of micrometer in width and depth, the component rearrangement approaches described above are usually unsuccessful. Given this, the film needs to be thicker, and the regeneration should also include healing of the bulk of the film, even in the area underneath the direct surface region.

One such example is reported by Wu et al., who prepared a conductive superhydrophobic film. The authors first coated a film of polycaprolactone (PCL)/poly(vinyl alcohol) (PVA) with a layer of Ag nanoparticles and Ag nanowires (AgNPs-AgNWs), and further modified with 1H,1H,2H,2H-perfluorodecanethiol (PFDT) to reduce the surface energy. The obtained film demonstrated superhydrophobicity with a water CA of about 158° and a rolling-off angle of 3° (volume of droplet, Vdrop = 4 μL). After being severely scratched, the liquid repellency loss of such a surface could be healed by employing voltage or near-infrared (NIR) light.[29] Taking advantage of the electrothermal and photothermal effects of AgNPs-AgNWs, the temperature of the surface would increase and induce the thermal healing of the PCL/PVA film when an electric current or NIR light is applied. With this approach, cuts in hundreds of micrometers wide could be healed rapidly and repeatedly, or at least the width of cuts be significantly narrowed down. They cut the PFDT/AgNPs-AgNWs/(PCL/PVA)*7 film with a knife, and the cut had a width of 136 μm and penetrated down into the underneath substrate (**Figure 9**a). The damaged area became sticky with a water droplet adhered even when it was turned upside down (Figure 9a, inset). The exposure of hydrophilic (PCL/PVA)*7 to the air caused such a change in wettability (Figure 9b). Superhydrophobicity could be recovered by treating the damaged film with a 4 V voltage (0.31 W cm^{-2}) for 1 min. As shown in Figure 9c, the cut became narrow with the superhydrophobicity healed. Water CA hysteresis and rolling-off angle were decreased to 2° and 3°. Magnified SEM image showed that the bottom of the cut was healed with the hierarchical structure of AgNPS-AgNWs (Figure 9d). However, when the cut was made perpendicular to the current direction, across the entire length of the prepared film, voltage treatment was ineffective since the top layer was no longer conductive. In this situation, NIR light was employed to trigger the healing process due to the photothermal effect of AgNPs-AgNWs. Figure 9e showed a cut with a 72 μm of width, which was across the entire length of PFDT/AgNPs-AgNWs/(PCL/PVA)*7 film. The damaged surface lost its superhydrophobicity (Figure 9e, inset). However, after irradiating the surface with 812 nm NIR light (≈1.4 W cm^{-2}) for 1 min, the separated film was reconnected with hierarchical structured AgNPs-AgNWs, and the superhydrophobicity was recovered (Figure 9f). The healing of physical damage was driven by the flow of thermally healable (PCL/PVA)*7 layer underneath the AgNPs-AgNWs texture (Figure 9g). When a voltage or NIR light is applied, the AgNPs-AgNWs act as an electrothermal or photothermal heater, which can efficiently convert the electrical energy or light into thermal energy, and heat up the (PCL/PVA)*7 to its melting temperature. Then the molten film will flow to the damaged region driven by capillary pressure to reduce the surface energy. As a result of the strong adhesion between the PFDT/AgNPs-AgNWs layer and the (PCL/PVA)*7 film, the flow of (PCL/PVA)*7 film pulls the separated PFDT/AgNPs-AgNWs layers towards each other, resulting in the full healing or greatly narrowing the severe scratches and recovering the superhydrophobicity.

Similarly, Qin et al. reported a conductive self-healing superhydrophobic conductor which could heal the surface wettability by applying a voltage after the surface was severely damaged.[30] First, a mixture of $FeCl_3$, acetylene black (AB), and gallic acid (GA) modified PDMS was molded to obtain a PDMS-GA conductor. Then, TiO_2 nanoparticles (≈200 nm in diameter) and super P (≈50 nm in diameter) were dropped on the surface of PDMS-GA conductor to form a composite conductor. Finally, the composite conductor was modified with 1H,1H,2H,2H-perfluorodecyl triethoxysilane (PFDS) to minimize surface energy. The as-prepared conductor presented superhydrophobicity (water CA of 155° and a CA hysteresis of 3°) and a fast self-healing behavior driven by direct current (DC) power. As shown in **Figure 10**a, the superhydrophobic conductor was cut into half with a razor blade, and then the pieces were aligned for a geometric match and subjected to 10 V DC power. After only 1 min treatment, the two halves coalesced back into one entire piece which could support its own weight, indicating the successful healing of the macroscopic configuration. Meanwhile, the superhydrophobicity was also recovered. Water droplet performed a CA of about 155° and could be easily rolled off at the healed region (Figure 10b). SEM characterization confirmed that the healing process was efficient. There were almost no cracks in the healed region (Figure 10b, inset). Uniaxis tensile experiments showed that the healed conductor shows a tensile strength of 467.2 ± 7 kPa, which was around 86.4% of the original equivalent. In addition, the breaking elongation also recovered about 73.3%, indicating the effective self-healing behavior of the superhydrophobic conductor. The superhydrophobicity and mechanical properties could be effectively healed within six cycles of cutting/healing (Figure 10c). The healed conductor maintained a water CA above 153° and a tensile strength up to 448.7 ± 8.7 kPa after the sixth restoration. Such highly efficient healing behavior of the conductor was derived from the temperature-dependent dynamic pyrogallol-Fe coordination. As shown in Figure 10d, once the aligned halves were subjected to

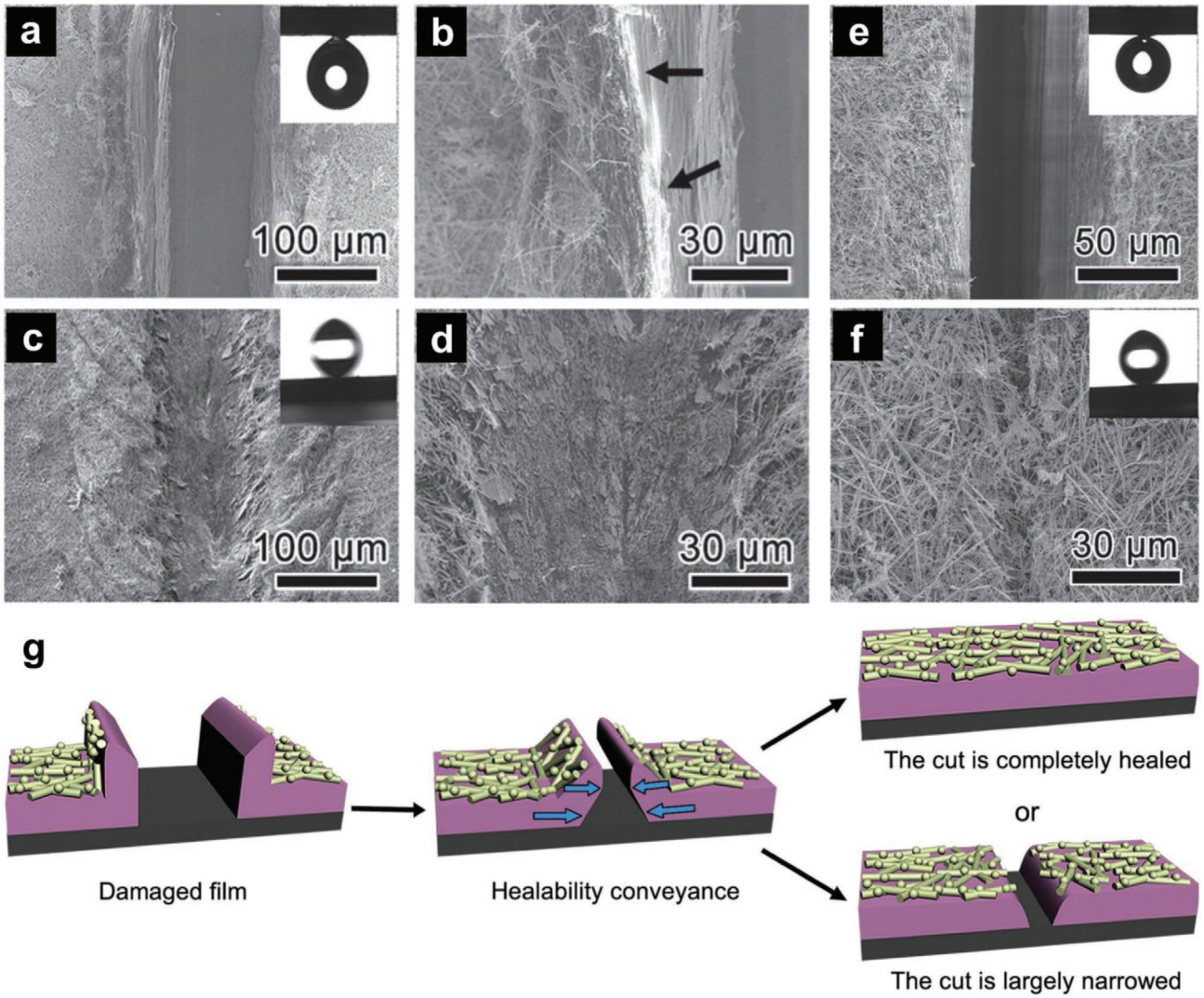

Figure 9. a–d) SEM images of the PFDT/AgNPs-AgNWs/(PCL/PVA)*7 film with a ≈136 μm wide-cut before (a,b) and after (c,d) being healed by applying a voltage of 4 V. a) The cut film. b) Magnified SEM image of the edge of the cut shown in (a), indicating the exposed (PCL/PVA)*7 film. c) The cut film in (a) after being healed. d) Magnified SEM image of the healed area of the film. e,f) SEM images of a PFDT/AgNPs-AgNWs/(PCL/PVA)*7 film with a ≈72 μm wide-cut before (a) and after (b) being healed by an 812 nm NIR light irradiation. g) Schematic illustration of the healability conveyance process for restoring superhydrophobicity of the PFDT/AgNPs-AgNWs/(PCL/PVA)*7 film. Insets in the SEM images show the shape of a water droplet poisoned on the damaged region of the film before and after applying voltage or NIR light. a–g) Reproduced with permission.[29] Copyright 2016, Wiley-VCH.

DC power, their bulk temperature would increase to 155 °C in a short time due to the Joule thermal effect. The elevated temperature weakened the coordination between pyrogallol moiety and Fe^{3+}, allowing part of the PDMS-GA chains to be released from the cross-linked network. The free PDMS-GA chains were able to move across, entangle, or interpenetrate at the contact interface of the aligned halves. Then new bis-pyrogallol-Fe complexation formed between the entangled chains, resulting in the healing of the broken PDMS-GA network. Since TiO_2 and super P nanoparticles were integrated into the PDMS-GA network, the healing of the beneath network could drive the rearrangement of nanoparticles and regenerate the rough hierarchical structures, resulted in the recovery of the superhydrophobicity. Such simple electrical induced fast self-healing of superhydrophobic surface efficiently avoids traditional stimuli, for example, light, pH, and organic solvents, making it possible to meet the requirement in applications like self-cleaning, anti-icing, advanced electronic, and so on. In general, the regeneration of hierarchical topography by using self-healing materials radically enhances the performance of superhydrophobic surfaces then exposed to harsh environments.

Another approach for topography regeneration is relied on shape memory polymers (SMP). SMP are stimuli-responsive materials that can restore their original morphology from temporarily deformed shapes by an external stimulus. Employing such kind of material for superhydrophobic surface preparation can completely heal the deformed structure.[31]

Using SMP as building materials, Zhang et al. fabricated pillar arrays based on self-healing superhydrophobic surface by polymerizing prepolymer in a PDMS mold.[32] The obtained

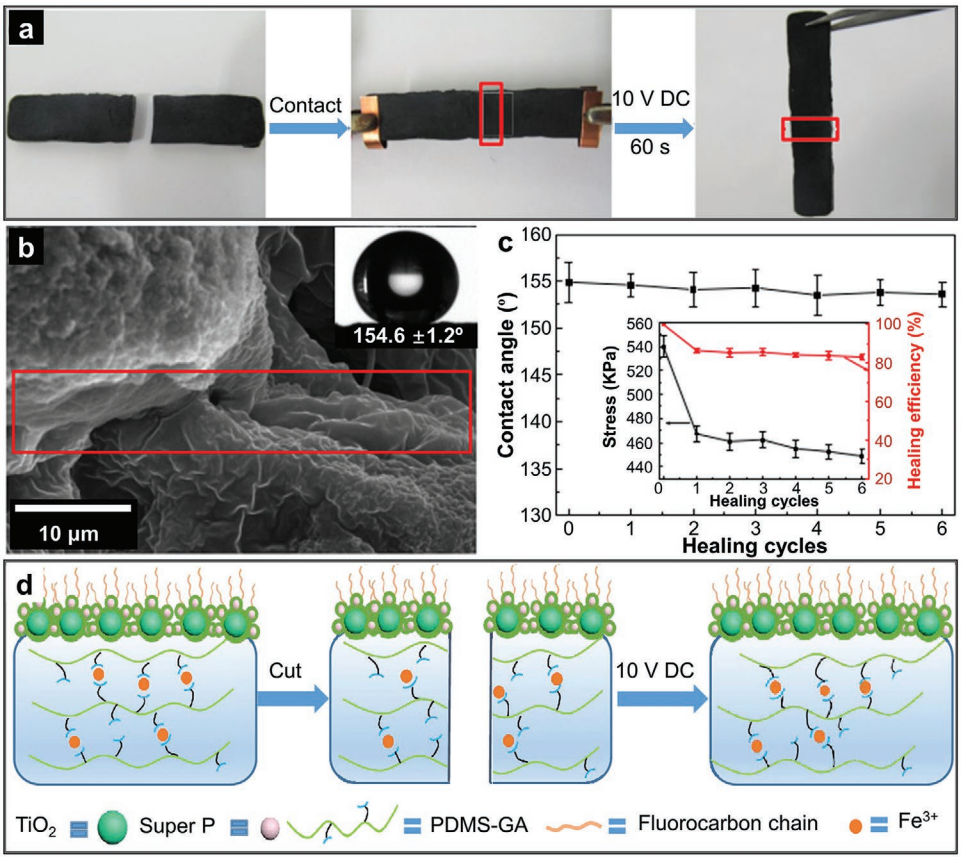

Figure 10. a) Photographs show cutting and self-healing of the superhydrophobic conductor. b) SEM image of the healed region (red rectangle). Inset is a water droplet placed on the healed region. c) Variation of WCA after multiple cutting/healing cycles. Inset is the tensile stress and mechanical healing efficiency during the cycles. d) Illustration schematics of the restoration mechanism of the superhydrophobic conductor. a–d) Reproduced with permission.[30] Copyright 2019, American Chemical Society.

surface was uniformly coated with regular pillars with the diameter and spacing of about 3 and 10 μm (**Figure 11**b). Due to the high aspect ratio pillars that provided high air/liquid areal fraction and the low-surface energy components mixed in the structure, the achieved surface demonstrated superhydrophobicity with a 6 μL water droplet CA of 156° and a rolling-off angle of 5° (Figure 11c). When the regular vertical pillars were deformed by pressing, collapsed pillar structures were observed (Figure 11d). Due to the decrease of air/liquid areal fraction, water droplet with the same volume was pinned on the surface with an apparent CA of 111°, indicating superhydrophobicity loss (Figure 11e). After heating the deformed surface at 120 °C for 343 s, the collapsed pillars recovered the initial upright state (Figure 11f), accompanied by the recovery of superhydrophobicity. Taking advantage of the structural restoration-induced self-healing process, one can easily control the surface wettability. As shown in Figure 11a, the authors prepared a patterned surface that combined collapsed and vertical pillars by pressing the surface with a patterned template. Dot structure with a diameter of about 0.1 mm was obtained with the inner part constructed by collapsed pillars while the outer region remained the upright state (Figure 11g–i). Water droplets deposited on the patterned region were pinned with a CA of 153° even turned the substrate upside down (Figure 11j), indicating that after introducing microscale patterns, high adhesive superhydrophobic wetting performance could be obtained. When the surface was heated at 120 °C for 343 s, the collapsed pillars were recovered to the vertical state, resulting in the removal of microstructure and transformation of low adhesive superhydrophobicity. Such low adhesive rolling ability and high adhesive pinning feature could be repeatedly switched for many cycles, further confirmed the excellent self-healing behavior of the surface (Figure 11k, SA = 90° represents the pinning state).

Similarly, Chen et al. also fabricated a self-healing superhydrophobic surface based on high aspect ratio micropillar arrays.[33] The micropillar arrays performed a square lattice arrangement, with each micropillar having an aspect ratio of 3 (**Figure 12**). The large spacing between pillars provided a high air/liquid areal fraction, which resulted in a superhydrophobicity with water CA reaching 155° (inset of Figure 12a). When the vertical micropillars deformed, water droplets changed to a Wenzel state accompanied by the loss of superhydrophobicity (Figure 12b). After heating the deformed surface at 80 °C (above the Tg of the SMP of ≈60 °C) for about 50 s, the deformed micropillar structure was recovered to the original vertical morphology with a square lattice arrangement. Meanwhile, water droplets recovered the Cassie–Baxter mode with the superhydrophobicity regained as well (Figure 12c).

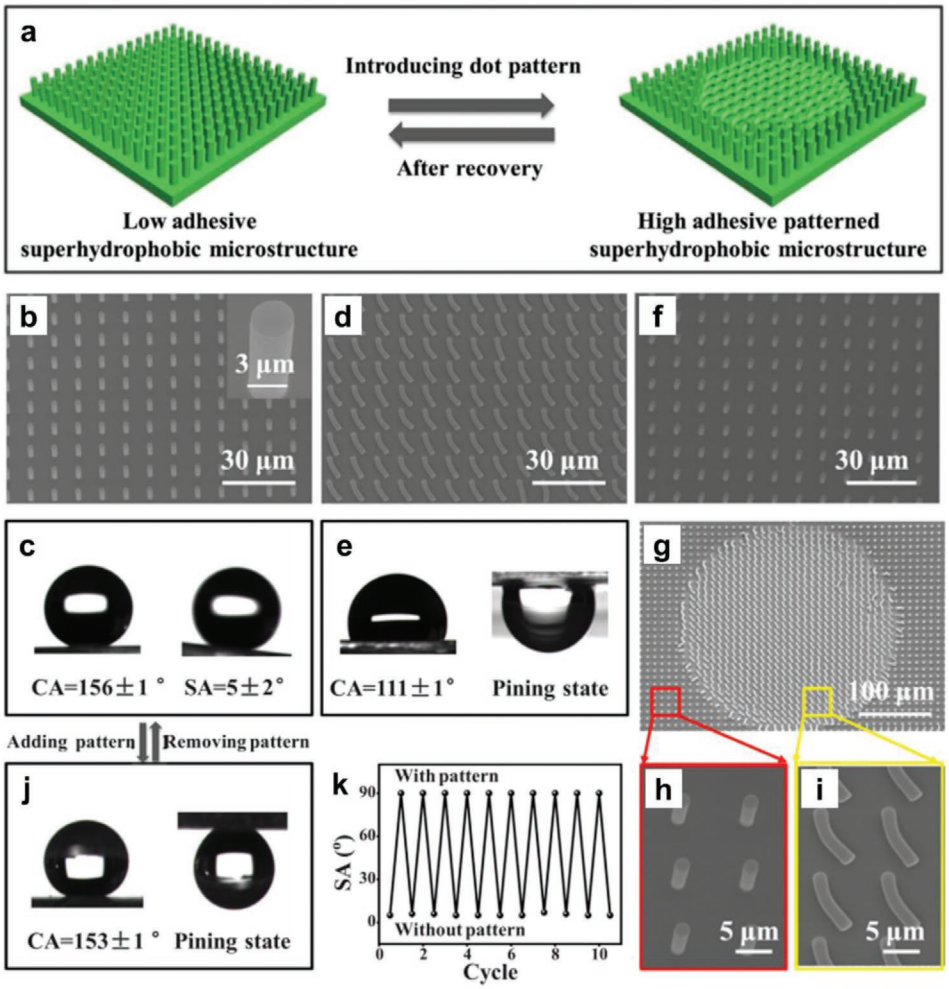

Figure 11. a) Schematic illustration of the wetting/adhesion control by introducing/removing dot patterns on the superhydrophobic SMP surface. b,d,f) are SEM images of the initial surface, the surface after pressing by a flat glass side, and the recovered surface, respectively. Inset in (b) is the magnified image of one pillar. c,e) show shapes of a water droplet standing and rolling on the surface corresponding to (b), and (d), respectively. g) SEM image of the patterned surface with dot shape, h,i) are enlarged images corresponding to different regions as marked in Figure (g). j) Images of a water droplet on the patterned surface titled at 0°, and 180°, respectively. k) Reversible low/high adhesion transition can be achieved several times by repeatedly introducing/removing dot patterns. a–k) Reproduced with permission.[32] Copyright 2020, Elsevier.

Since high aspect ratio pillars are usually mechanically unstable and unfavorable for dynamic control, Lv et al. reported a superhydrophobic surface based on epoxy SMP micropillar array with an aspect ratio of 1.[34] Water droplets on the as-prepared surface performed a CA of about 151° (Figure 12i,l). Once the surface was deformed by heating and mechanically pressing, the water CA reduced to 110° (Figure 12j,m). The superhydrophobicity could be recovered by heating the deformed surface at 120 °C for about 45 s. The original micropillar structure was restored, and the water CA was recovered to 151° (Figure 12k,n). As a result of the low aspect ratio of the achieved micropillar arrays, such superhydrophobic surface demonstrated enhanced durability with both the micropillar structure and superhydrophobicity could still be restored after 50 cycles of the deforming-healing process (Figure 12o). Guo et al. fabricated a robust self-healing superhydrophobic surface by aerosol-assisted layer-by-layer chemical vapor deposition of epoxy resins and PDMS polymer films.[35] Attributed to the coordination of micro-nano hierarchical structures and the low-surface energy of PDMS, the obtained surface performed superiorly stable superhydrophobicity (water droplet (7 μL) CA of 164° with rolling-off angle 2°) with its superhydrophobicity maintained even after being irradiated with UV for 168 h, peeled with double tape for 200 cycles, abraded with sandpaper for 2 meters with 100 g weight loaded, and immersed in strong acid/base for 72 h. Benefit from the shape memory effect of epoxy resin, the micro-nano hierarchical structure could be fully recovered after damaged by external load and followed by the regeneration of its superhydrophobicity.

In addition to the above-mentioned superhydrophobic surfaces, Wang et al. developed the first superamphiphobic SMP surface, which was not only able to repel water but also oils.[36] Using thiol-ene/acrylate-based thermos-responsive SMP as a building material, mushroom-like structures with re-entrant features were achieved by a combination of photolithography and reactive ion etching (Figure 12d). Superamphiphobicity was

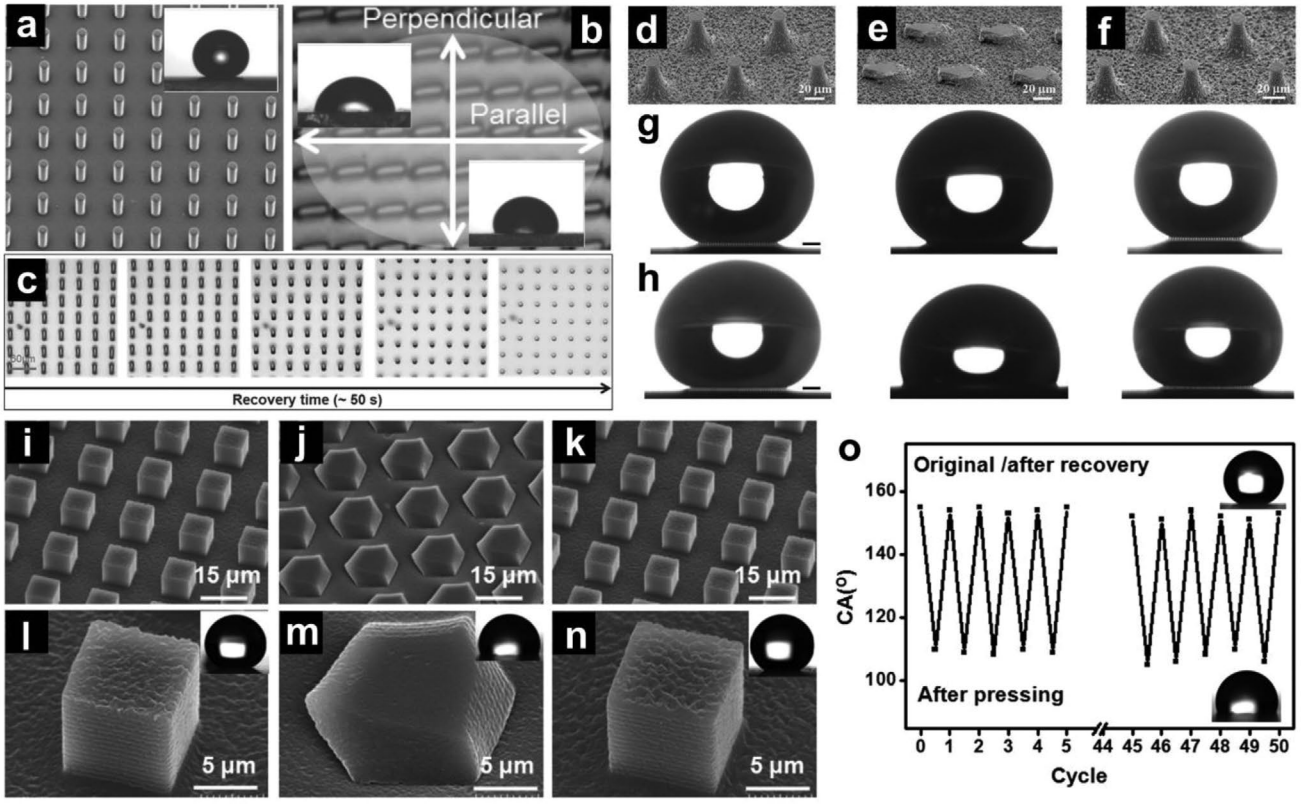

Figure 12. a) SMP micropillar-based superhydrophobic surface; b) Deformed pillar structure; c) Morphology recovery of deformed pillars under 80 °C. Insets show the photographs of water droplet in different state. a–c) Reproduced with permission.[33] Copyright 2013, Wiley-VCH. d–f) SEM images of SMP pillars in the d) original, e) deformed, and f) recovered morphologies. g,h) Water (g) and *n*-hexadecane (h) droplets on the surface corresponding to different pillar morphologies. d–h) Reproduced with permission.[36] Copyright 2017, Wiley-VCH. i–n) SEM images of SMP micropillar-based superhydrophobic surface viewed at a tilt angle of 40°: i,l) The original achieved structure; j,m) Deformed pillar structure; k,n) Morphology recovery of deformed pillars under 120 °C. Insets show the photographs of water droplets in different states. o) Change in water CA of the pressed and self-recovered surface. i–o) Reproduced with permission.[34] Copyright 2016, American Chemical Society.

obtained after coating the structure with low-surface energy molecule, heptadecafluoro-1,1,2,2-tetrahydrodecyl trichlorosilane. The prepared SMP surface demonstrated a similar morphology recovery behavior as the above-mentioned epoxy SMP surface. The mushroom-like structure could be reversibly switched between the original morphology and the deformed shape through pressing-healing processes (Figure 12e,f). The original low adhesive Cassie–Baxter state could be recovered for both water and *n*-hexadecane but showing different wetting switching behaviors (Figure 12g,h). In the deformed state, hexadecane wets the surface and reveals a Wenzel state. In contrast, the water droplet maintained the Cassie–Baxter state even on the deformed surfaces. On the deformed surface, the loss of reentrant structure showed an insignificant effect on the water wetting state. However, *n*-hexadecane absorbed into the structure and finally transformed the oil into the Wenzel state.[31a] The excellent controllability of the mushroom-like structure and surface wettability endowed the prepared surface with great potential in rewritable liquid patterns, and biosensors.

Besides using stimuli-responsive SMP as building materials, Das et al. reported a robust and self-healing bulk-superhydrophobic surface.[37] The superhydrophobic surface was obtained by a 1,4-conjugate addition reaction between aliphatic primary amine groups provided by branched poly (ethylenimine) (PEI) and amino-graphene oxide (AGO), and the aliphatic acrylate groups provided by dipentaerythritol penta-acrylate (5Acl). The combination of random aggregation of granular polymer domains and AGO sheets formed porous topography provided the structural necessity for superhydrophobicity. After modified the residual acrylates groups with decylamine molecules, the surface demonstrated an advancing water CA of 162° and CA hysteresis of 3°. After pressing the coating with a 188 kPa of pressure, the porous structure was deformed, resulting in superhydrophobicity loss. The original nonadhesive superhydrophobic surface turned to highly adhesive with a CA hysteresis of 50°. However, the deformed surface could be self-regenerated by exposed to an ambient environment for one day after the pressure was released. The self-healing behavior could be repeated for 40 cycles of damage-recovery processes, and such self-healing could be sped up by increasing the amount of AGO in the coating. When the concentration of AGO reached 30.8 μg mL^{-1} in the coating solution, the complete healing was finished within 30 min under ambient conditions. The fast and revisable recovery from adhesive wetting state to nonadhesive repellency endowed it with the ability to develop rewritable aqueous patterns on the extremely water repellent polymeric

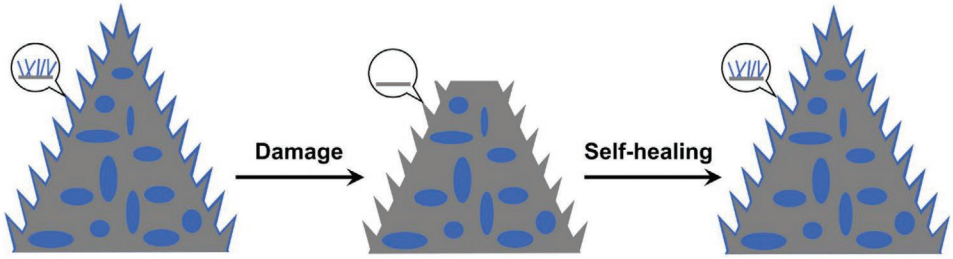

Figure 13. Self-healing principle of superhydrophobic surfaces based on the coordination of low-surface energy substances transportation and rough topography regeneration. Blue represents the low-surface energy substances; gray represents the basic physical structure.

coating. This kind of stimuli-free self-healing of topography opens a new direction for self-healing superhydrophobic surface fabrication, which will greatly contribute to the practical application of superhydrophobic surfaces with a simple surface healing process.

2.3. Coordination of Low-Surface Energy Materials Transportation and Rough Topography Regeneration

Besides using either low-surface energy materials transportation or rough topography regeneration, researchers also tried to combine these two strategies to develop self-healing superhydrophobic surfaces, which can meet the requirements to repair both physical and chemical damages (**Figure 13**).[38]

Several superhydrophobic surfaces have been developed based on the above self-healing principle. Wang et al. fabricated a superamphiphobic surface by coating a fabric substrate with fluoroalkyl surface-modified silica nanoparticles (FS-NP) followed by a second step coating of a mixture of tridecafluorooctyl triethoxysilane (FAS) and fluorinated decylpolyhedral oligomeric silsesquioxane (FD-POSS).[39] The obtained surface presented excellent liquid repellency. 10 µL of water, hexadecane, and anhydrate ethanol droplets deposited on the surface performed spherical morphology with CAs of 171°, 157°, and 151°, respectively. After treated with air-plasma to generate polar groups, the low-surface energy substances were decomposed. The superamphiphobic surface turned amphiphilic, with CAs of 0° for both water and oil. The degraded surface could be healed after heating at 140 °C for 5 min. High temperature accelerated the mobility of FAS persevered in the coating, which transported to the damaged area to minimize the surface energy. Meanwhile, SiO_2 nanoparticles greatly reduced the plasma etching effect for organic materials, protecting the beneath FD-POSS/FAS. The superamphiphobicity could be regained even after 100 cycles of plasma etching and heating. Moreover, the surface repellency could be recovered after degraded by physical damage. After heating at 140 °C for 30 min, the FD-POSS and SiO_2 nanoparticles could reconstruct the surface roughness damaged after abraded with a 1200# sandpaper. Such topological rearrangement led to superamphiphobicity recovery. Benefit from structure regeneration, the superamphiphobicity of the surface could still be maintained after 2000 cycles of abrasion and recovery. Using epoxy-based SMP, Lv et al. also achieved a superhydrophobic surface that could recover from both surface structure deformation and surface chemistry degradation.[40] The recovery process of the deformed or damaged surface was triggered by heating. Chemical damage was healed by the transportation of low-surface energy polymer chains to the polarized surface to minimize the low-surface energy. Meanwhile, the deformed hierarchical structure could also be regenerated due to the thermal-responsive SMP. It could be transformed from its temporary shape back to its permanent structure upon heating treatment. Restoration of both chemical and physical damage could further improve superhydrophobic surfaces' durability while meeting the requirements posted by different internal and external conditions, resulting in a broader perspective of applications.

3. Applications of Self-Healing Superhydrophobic Surfaces

Being able to prepare self-healing super liquid-repellent surfaces with superior durability provides more possibilities for various practical applications. In this section, we offer an overview of typical potential applications of self-healing superhydrophobic surfaces.

3.1. Prevention of Corrosion

By directly modifying a surface with superhydrophobicity, and thus water repellency, we can greatly prevent or avoid the contact between water and the substrate, and therefore protecting the substrate from corrosion.

Yuan et al. fabricated anti-corrosion and self-healing superhydrophobic aluminum surfaces by combining femtosecond laser ablation and post-process heat treatment.[41] With the environmentally friendly femtosecond laser processing, microscale protrusions were fabricated on aluminum substrate, while the ablated nanoparticles and microparticles deposited on the microscale topology, forming hierarchical structures. Followed by a post-heating treatment to reduce the surface energy, the fabricated surface demonstrated superhydrophobicity. Water droplet posited on the surface performed a Cassie–Baxter wetting with a CA larger than 160° and a rolling-off angle smaller than 5°. Benefit from the water repellency, the as-prepared superhydrophobic surface showed good anti-corrosion property. After immersing the superhydrophobic sample and flat aluminum surface in 5 wt% $CuCl_2$ solution for 3 min, the flat aluminum was entirely covered with red copper (due to the

replacement reaction between aluminum and Cu^{2+}). However, no color change of the superhydrophobic surface was observed, meanwhile, the liquid repellency was maintained. The mechanism behind this is that the hierarchical structure on the surface endowed the substrate with a high air/liquid areal fraction, which formed an air pocket between microstructures, and prevented liquid contact with the solid substrate. Thus, the aluminum structure was prevented from contact with corrosion agents, resulted in an effective anti-corrosion.

Besides the above-mentioned superhydrophobic surface with direct contact of the metal structure and liquid or corrosion agent, an additional superhydrophobic coating on the metal surface could perform a better anti-corrosion behavior, since the metal substrate and corrosion agent are separated by the superhydrophobic coating. Based on this idea, Zhao et al. prepared a self-healing superamphiphobic coating for efficient corrosion protection of magnesium (Mg) alloy.[42] In their work, a self-healing epoxy resin (SHEP) coating with a thickness of 130 ± 5 μm was first prepared onto Mg alloy. And then a layer of perfluorodecyl polysiloxane modified silica nanoparticles (PF-POS@silica) with a thickness of 142 ± 1.5 μm was spray coated onto the SHEP surface, forming a SHEP/PF-POS@silica coating. The hierarchical structure constructed by silica nanoparticles and the low-surface energy of fluorodecyl polysiloxane endowed the composite surface with superamphiphobicity. 3.5 wt% NaCl droplet showed a CA of 166° with a rolling-off angle of about 2°, while *n*-hexadecane droplet performed a CA of 160° with a rolling-off angle of 4°. Due to the superamphiphobicity of silica coating and the compactness of the SHEP layer, air pockets trapped in between silica hierarchical structure will prevent the penetration of liquid or corrosion agent, resulting in the corrosion protection of the coated Mg alloy. The anti-corrosion performance was conducted by immersing Mg alloy and SHEP/PF-POS@silica coated Mg alloy in 3.5 wt% NaCl. For Mg alloy without any protection, the corrosion potential and corrosion current density were –1.505 V and 7.85×10^{-5} A cm^{-2}, respectively, suggesting fast corrosion. But for SHEP/PF-POS@silica coated Mg alloy, these values reduced to –1.112 V and 5.971×10^{-12} A cm^{-2}, indicating that the superamphiphobic surface possessed an excellent anti-corrosion behavior. It is worth noting that, after immersing the SHEP/PF-POS@silica coated Mg alloy in corrosion agent for 408 h, no evident corrosion happened. Moreover, due to the shape memory effect of the epoxy polymer, the SHEP coating could be self-healed with heat treatment after the coating was mechanically damaged. The repair of SHEP coating could drive the arrangement of the silica nanoparticles on top to restore the hierarchical topology, resulted in the self-healing of superhydrophobicity, which further prolonged the durability for long-term anti-corrosion applications.

Ezazi et al. prepared a self-healing superamphiphobic surface for corrosion protection.[43] In their work, a cross-linked mixture of epoxidized soybean oil, perfluorinated epoxy, citric acid, and silica nanoparticles was spray-coated on a copper mesh. The obtained surface was superamphiphobic with a 3 μL *n*-dodecane droplet presented a CA of 151° and a rolling-off angle below 10°. Benefit from such liquid repellency, the coated surface demonstrated good corrosion protection performance. The corrosion rate of the superamphiphobic surface was only about 20% of the normal superhydrophobic anti-corrosion coating when immersed in corrosion agent (3.5 wt% NaCl aqueous solution). The diffusion of corrosion agent into the coating was significantly prevented with complete saturation after 108 h. In contrast, when using commercial paint, it took only 0.3 h. Importantly, when the surface was mechanically damaged, the loss of water repellency and anti-corrosion was automatically healed after heating the surface at 60 °C for 1 min, indicating an efficient, long-term corrosion protection performance.

When a corrosion inhibitor was preserved inside the self-healing superhydrophobic coating, enhanced anti-corrosion behavior could be obtained. Qian et al. fabricated a self-healing superhydrophobic surface which possessed an anti-corrosion property.[31c] The superhydrophobic surface was fabricated on a steel substrate based on the replication of a lotus-like structure using epoxy-based SMP. The obtained hierarchical structure was integrated with corrosion inhibitor, benzotriazole (BTA). Attributed to the shape memory property of SMP, a mechanical scratch caused surface damage could be easily recovered after short heating treatment, resulted in a prolonged anti-corrosion durability. The preserved BTA can leach to the scratch area and inhibit the corrosion of the exposed substrate, further decreasing the corrosion rate to about 10% compared to the SMP coated steel substrate without BTA preserved. Similarly, Ding et al. developed a superhydrophobic coating based on mechanized silica nanoparticles for reliable protection of magnesium alloys.[44] The anti-corrosion coating was achieved by coating a mixture of mechanized silica nanoparticles (MSNPs) with corrosion inhibitor (2-hydroxy-4-methoxy-acetophenone, HAMP) preserved and self-assembled silica nanoparticles, followed by a modification of PFDS. Here, the nanoparticles offered structural necessity, while PFDS endowed the coating with low-surface energy. The HAMP persevered in the MSNPs was released upon alkali or Mg^{2+} stimuli produced by the corroding micro-regions of magnesium alloy. The coordination of corrosion inhibition properties of the released HAMP and the recoverable superhydrophobicity due to the self-healing ability of the coating, led to long-term anti-corrosion behavior.

3.2. Oil/Water Separation

Utilizing the (super) oleophilicity property of superhydrophobic surface to penetrate oil while intercepting water. Self-healing superhydrophobic surface could be applied in oil/water separation for environmental protection and resource preservation.

Zhu et al. achieved a self-healing superhydrophobic material by coating a copper mesh (copper mesh (copper fiber with a diameter of 30 μm forming square holes in size of 30 μm × 30 μm) with a mixture of TiO_2 nanoparticles and PDMS.[45] With the help of the hierarchical structure formed by the assembly of TiO_2 nanoparticles and the low-surface energy of PDMS, the coated mesh demonstrated superhydrophobicity with a water CA of about 156° and a rolling-off angle of about 7°. Here, besides providing low-surface energy, PDMS also acted as a self-healing agent after the surface being chemically damaged and an adhesive to connect TiO_2 nanoparticles and fix them on the mesh to form stable structures. Once the surface was degraded by O_2 plasma treatment, the embedded

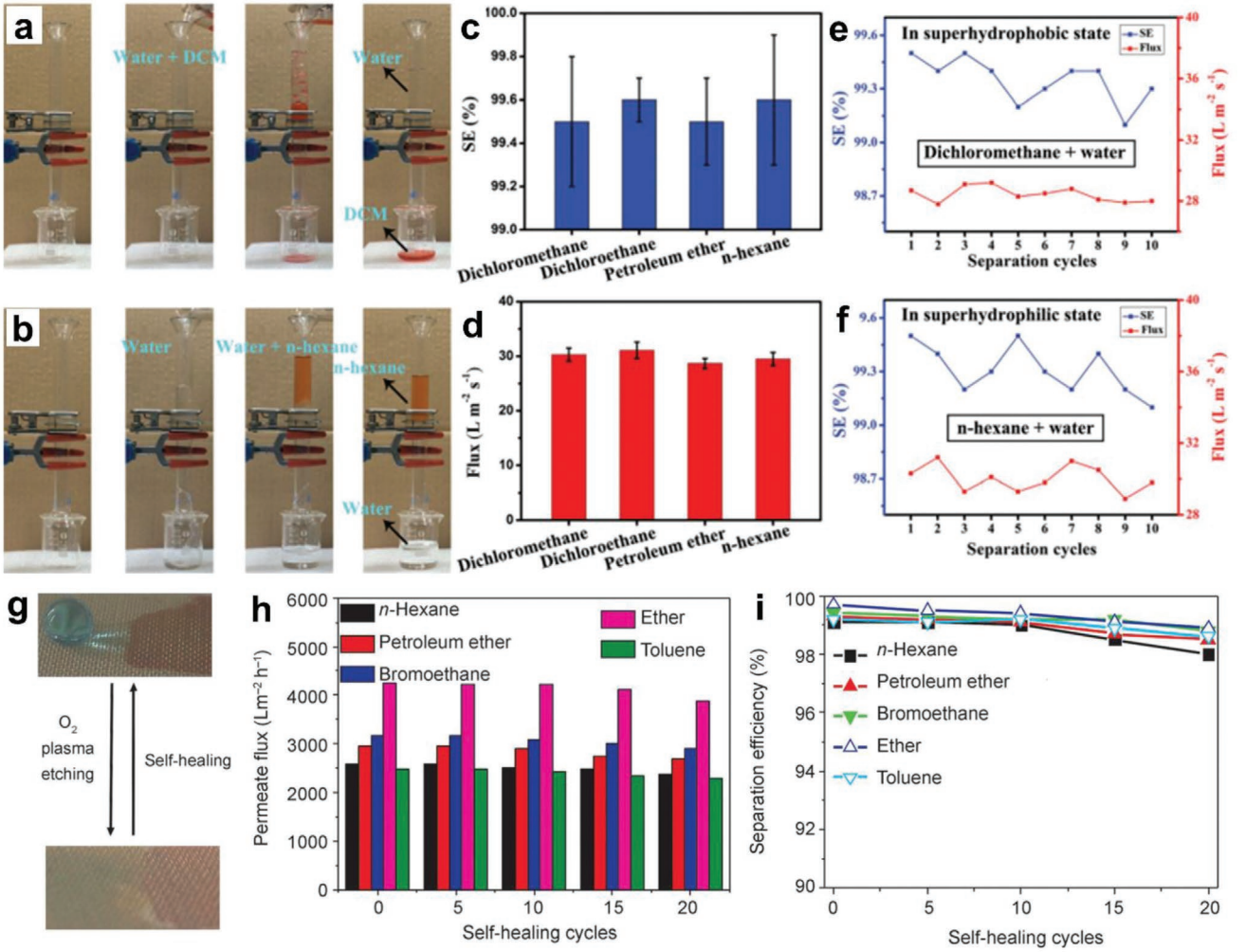

Figure 14. a) Heavy and b) light oils are separated from oily wastewater. c) SEs of oily mixtures by superhydrophobic P25@PDMS@COM. d) Fluxes of oily mixtures by superhydrophilic P25@PDMS@COM after O_2 plasma treatment. Separation cycles of e) DCM, f) *n*-hexane and water by P25@PDMS@COM, where SEs and fluxes are shown. a–f) Reproduced with permission.[45] Copyright 2020, Royal Society of Chemistry. Self-healing and oil-water separation behavior of membrane (PU-C8F17/PU-C18H37 = 2:1) g–i). g) CA reversible transition upon O_2 plasma-and-heating cycles, water and oil are dyed by methyl blue and sudan III, respectively; h,i) permeate flux and separation efficiency of the membrane (PU-C8F17/PU-C18H37 = 2:1) after 20 self-healing cycles. g–i) Reproduced with permission.[47] Copyright 2016, Wiley-VCH.

PDMS chains could transfer to the damaged surface to reduce the surface energy, endowing the surface with self-healing property. Taking advantage of the reversible variation of the surface wettability, the as-prepared surface could be used for complex oil/water separation. In the superhydrophobic state, the surface could be used for separating heavy oils (dichloromethane and dichloroethane) from water. Oil could infiltrate the coated mesh quickly while water was retained on the top (**Figure 14**a). Once the surface was treated with O_2 plasma to change the superhydrophobicity to superhydrophilicity, the surface could be prewetted with water and used for separating light oils (petroleum ether and *n*-hexane) from water (Figure 14b). In this case, the prewetted superhydrophilic surface demonstrated an underwater superoleophobicity with an underwater oil droplet maintained a spherical shape and demonstrated a CA larger than 150°. Thus, water could easily go through the superhydrophilic mesh with the oil was blocked and retained on the top. In both of the above-mentioned wetting states, the separation efficiency was above 99.4%, meanwhile, the flux was about 30 L m^{-2} s^{-1}. These values maintained even after 10 separation cycles, indicating the fast and high efficient oil/water separation performance of the coated mesh (Figure 14c–f). In addition, due to the self-healing property, the surface could be easily transformed for either heavy oil or light oil separation, which made the coated mesh more promising for practical applications.

Similarly, Liu et al. achieved superhydrophobic fabrics with self-healing and high oil/water separation performance.[46] In their work, polyethylene terephthalate fabrics were coated with silica nanoparticles, which provided surface roughness, and self-healing silicon rubber reduced the surface energy and severed as a healing agent. The modified fabric performed superhydrophobicity with a water CA of 158° and high oil/water separation efficiency (≈99%). After the coating was damaged,

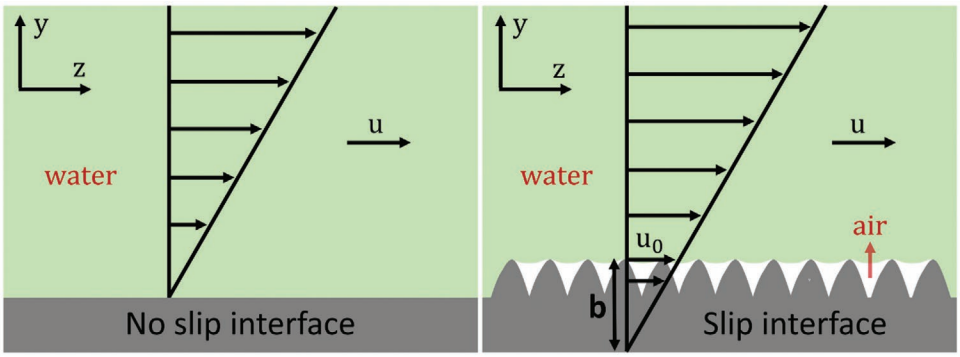

Figure 15. Schematic diagram of the slip boundary. Reproduced with permission.[50] Copyright 2019, American Chemical Society.

the modified fabric enabled fast self-healing at room temperature (in 10 min) and maintained the oil/water separation efficiency above 98%.

Besides coating fabrics, superhydrophobic membranes can also be prepared by electron-spinning polymers that possess low-surface energy for oil/water separation. Fang et al. reported a superhydrophobic membrane prepared by electron-spinning of synthesized *N*-perfluorooctyl-substituted polyurethane (PU-C_8F_{17}).[47] With such a superhydrophobic surface, mixtures of organic liquids with a surface tension lower than 30 mN m^{-1} (e.g., *n*-hexane, petroleum ether, bromothane, ether, and toluene) and water with a volume ratio (V_{oil}:V_{water}) of 1:1 could be successfully separated. Due to the high porosity of the electrospinning membrane, oils performed a large flux permeating through the membrane with the average value of 2580, 2962, 3165, 4253, and 2483 L m^{-2} per h, respectively (Figure 14h). Meanwhile, the membrane showed high separation efficiency for the above-mentioned oil/water mixture (99.2%, 99.4%, 99.5%, 99.7%, and 99.2%, respectively) (Figure 14i). The superhydrophobic membrane also presented self-healing abilities (Figure 14g). When the surface was treated by abrasion or plasma treating, the damaged liquid repellency could be healed by heating the membrane at 50 °C, with the oil/water separation ability maintained. The separation efficiency of oils was still above 98% even after 20 cycles of plasma damaging-heating. Such kind of superhydrophobic membrane also showed an excellent water-in-oil emulsion separation with an efficiency of 99.3%. Such efficiency slightly reduced to 98.1% after 20 cycles of plasma damaging–heating processes. The superior separation efficiency and durability make the superhydrophobic membrane great promise in oil/water separation.

3.3. Drag Reduction

Another considerable application field of superhydrophobic surfaces is drag reduction at low flow speed. Especially for thin channels or capillaries, high energy is usually required when pushing through the liquid. Therefore, drag reduction during the process has become an essential issue with the aim of energy saving. Due to the Cassie–Baxter wetting, there is an air layer between the liquid and solid surface retained when liquid flows over a superhydrophobic surface, while shear stress cannot be sustained for a free liquid surface. Thus, the usual no-slip boundary condition is replaced at the solid-liquid interfaces, resulting in drag reduction.[48] Slip can be quantified by slip length (**Figure 15**). The slip length b is related to the flow velocity at the interface by u_0:

$$u_0 = b\left|\frac{\partial u}{\partial y}\right| \tag{1}$$

The appearance of the finite value of b indicates the existence of a slip speed at the boundary. When performing Cassie–Baxter state on superhydrophobic surface, there is an air layer formed between the liquid and solid phases. Such formed air layer substitutes a liquid–gas interface for the liquid–solid surface when depositing liquid on superhydrophobic surfaces, inducing the free movement of the liquid at the contact interface. The generated effective slip during this process resulted in flow resistance reduction, indicating the drag reduction property of superhydrophobic surfaces.[48e,49] However, such effect of the surface is dramatically reduced as soon as destroyed by mechanical damage or contamination, which is inevitable. Therefore, superhydrophobic surfaces with integrated self-healing properties are promising candidates for long-term drag reduction.

Liu et al. achieved a self-healing superhydrophobic surface for drag reduction by hot-pressing a resin matrix with fluorinated silica particles (F-SiO_2).[50] The processable epoxy prepolymer was first synthesized by modifying the soft monomer trimethylolpropane tris(3-mercaptopropionate) (TMPMP) with glycidyl methacrylate (GMA) via a thiol-ene click reaction. Then self-healing resin matrix was prepared by further mixing the prepolymer with disulfide bond contained curing agent, 4-aminophenyl disulfide (APDS). Finally, the surface achieved an excellent superhydrophobicity by hot-pressing the matrix and F-SiO_2 in turn. Water droplet (V_{drop} = 8 µL) deposited on the surface showed a CA of 164° with a SA of 2°. The drag reduction property of the surface was evaluated by characterization of friction torque on the rheometer. The formulation below shows the calculation for drag reduction:

$$\mathrm{DR} = 1 - \frac{M_{sa}}{M_{sm}} \tag{2}$$

M_{sa} and M_{sm} represent the torque of the superhydrophobic surface and smooth surface, respectively. Based on the difference

of friction torque between superhydrophobic and flat surfaces under different rotation speeds, the superhydrophobic surface can reach its maximum drag reduction proportion of 27.7%, indicating a significant drag reduction effect. No obvious change in drag reduction performance could be observed even after 50 and 100 rounds of abrasion-healing processes due to the demonstrated self-healing property, suggesting that the as-prepared superhydrophobic surface possesses a long-term drag reduction behavior.

Artificial micro- and nanostructures have also been fabricated to mimic the superhydrophobic surface in nature. Since both shark skin and Salvinia leaves presented a very good drag reduction property, Ahmmed et al. fabricated a superhydrophobic PTFE surface that integrated both shark skin and Salvinia leaf microstructures.[51] The drag reduction of the bioinspired superhydrophobic surface was tested in a closed channel with turbulent flow. The pressure drop tests showed that the superhydrophobic surface performed a significant drag reduction compared to the normal flat substrate. Similarly, Liu et al. reported a PDMS-based superhydrophobic surface that replicated shark skin structure and was further modified with PFMA rushes.[28] The obtained surface demonstrated a good self-healing property. The liquid repellency could be healed simply by immersing the surface in DMF solution the chemical damage of superhydrophobicity. The rotational viscometer measurement showed that up to 21.7% drag reduction could be achieved on this biomimetic surface. The superhydrophobicity and drag reduction properties are durable. After immersing in water for 10 days, the air layer between the liquid and the solid surface was maintained. Meanwhile, drag reduction measurement demonstrated an insignificant change, indicating the robust drag reduction effect of the fabricated superhydrophobic surface for long-term practical applications.

3.4. Anti-Icing

The low adhesion behavior and the extremely small contact area between water droplets and solid substrates propose the superhydrophobic surfaces as great candidates in the anti-icing process. Compared to conventional superhydrophobic surfaces which are usually fragile and easily deteriorated during the icing-melting cycles, self-healing superhydrophobic surfaces are more promising alternatives as durable anti-icing surfaces. For example, Qin et al. successfully fabricated a self-healing superhydrophobic surface with excellent anti-icing properties.[30] Superior to the pristine PDMS-GA film, the TiO_2 particle coated PDMS-GA film with a further modification of PFDS showed a much longer delayed formation of ice (a water droplet froze into an ice bead after cooling on the as-prepared surface for 430 s, while on pristine PDMS-GA film only 100 s). Meanwhile, the adhesion of the formed ice bead to superhydrophobic surface was greatly reduced compared to that on the pristine counterpart. Such excellent anti-icing property was attributed to the trapped air among hierarchical structures. These air pockets significantly reduced the contact area between the water droplet and solid surface, slowing down the heat transfer at the interface. Therefore, the formed ice on the superhydrophobic surface can be easily removed. Such particular surface also showed self-healing ability under physical or chemical damage. The liquid repellency could be easily recovered, together with the delayed ice formation and low adhesion properties. Another superhydrophobic surface with self-healing and anti-icing properties was achieved by Li et al. via spray coating substrate with a mixture solution of PU, and hexadecyl polysiloxane modified SiO_2 (SiO_2@HD-POS).[52] The surface demonstrated superhydrophobicity with a water CA of 164° and a SA of 4° (V_{drop} = 10 µL). Anti-icing behavior was explored by conducting static and dynamic experiments under outdoor environments (–15 °C, RH = 54%), and a delay of freezing water droplet was observed (**Figure 16**a–c). A hazy appearance of water droplet (60 µL) was found at 34 min 16 s and frozen accomplished after 41 min. In comparison, after 5 min 28 s, the water droplet on a bare glass slide already started to freeze and accomplished after 9 min 58 s (Figure 16a). These results clearly showed that the prepared superhydrophobic surface could delay ice formation for about 30 min even under extremely freezing conditions. Dynamic anti-icing was conducted by continuously dripping water from 1 cm height onto the 4° inclined surfaces. On a glass slide without coating, ice gradually formed at 0 min 23 s, and a large quantity of ice formed after 33 min (Figure 16c). In contrast, no ice formed on the superhydrophobic surface during the whole experiment, suggesting an excellent dynamic anti-icing behavior. Such better anti-icing performance in the dynamic experiment than in the static experiment is due to the low adhesion between the water droplet and the surface. The water droplets had already rolled off from the surface before meeting its freezing temperature. The obtained superhydrophobic surface demonstrated durable anti-icing properties even after 60 cycles of icing-melting processes (Figure 16d–f), indicating a superior long lifetime than other reported anti-icing coatings.[53]

Besides the applications mentioned above, self-healing superhydrophobic surfaces also show great potential in various fields such as water-energy harvesting,[54] solar steam generation,[55] (anti-)condensation,[56] superior microwave absorption,[57] and so on.[24e,58]

4. Conclusion and Outlook

During the last decade, significant improvements have been accomplished towards preparing self-healing surfaces with super liquid repellency (**Table 1**). The healing process is automatically triggered at room temperature or, in many cases, after exposure to an external stimulus. Integration of the self-healing property into the superhydrophobic surfaces significantly promotes application in various fields, for example, corrosion protection, oil/water separation, drag reduction, and anti-icing. Such durability improvement makes it possible for superhydrophobic surfaces to fulfill harsh practical requirements, expanding their outdoor application potentials. However, limitations are still left to be solved before applying superhydrophobic surfaces in realistic and practical ways.

I. Rigorous and sophisticated conditions are required to prepare self-healing superhydrophobic surfaces as reported before, such as layer-by-layer assembly or requiring inert

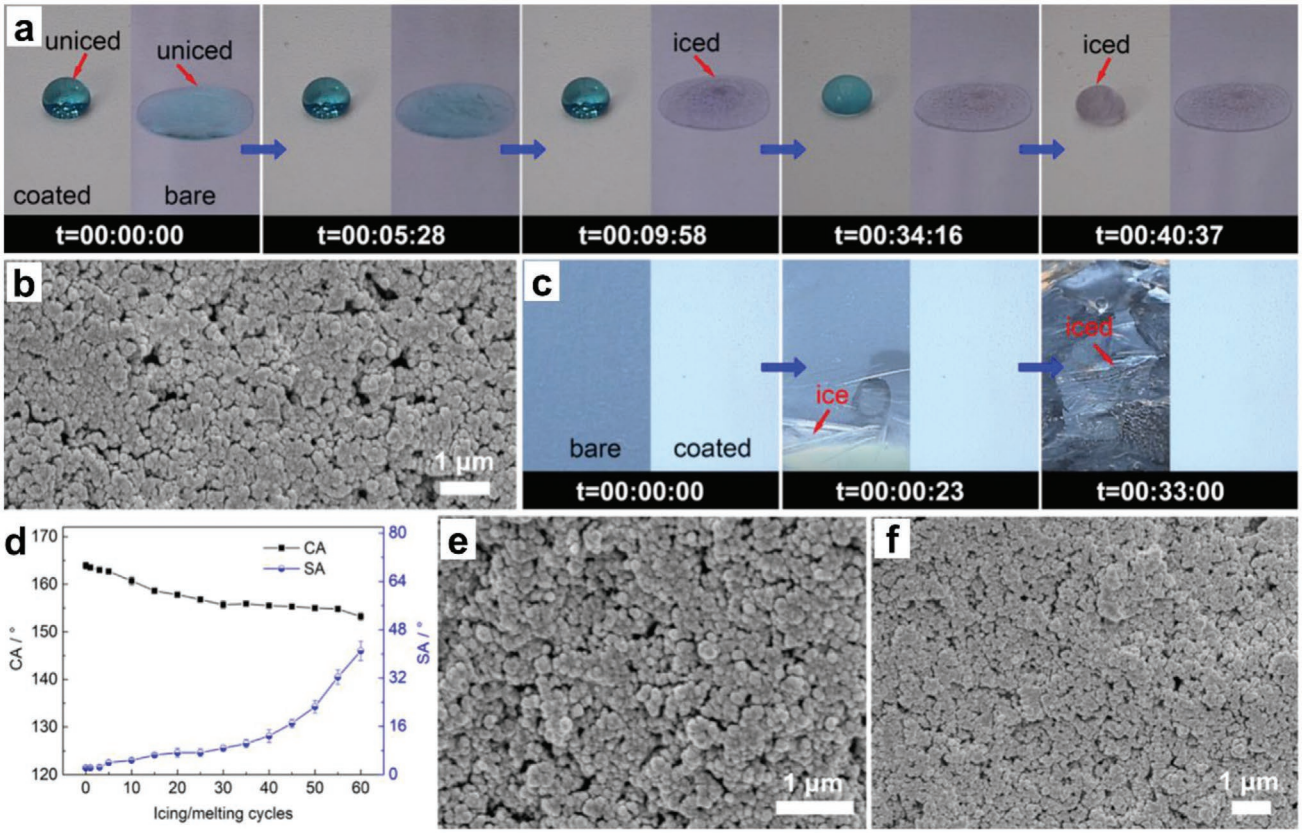

Figure 16. a) Photographs of the static icing process of water drops on the PU/SiO_2@HD-POS coating and bare glass slide. b) SEM photograph of the coating after the iced water drops are peeled off. c) Photographs of the dynamic icing process of water drops on bare glass slide and the coating. d) Changes of superhydrophobicity with icing/melting cycles. e,f) SEM photographs of the coating after 60 icing/melting cycles. a–f) Reproduced with permission.[52] Copyright 2018, American Chemical Society.

gas protection, these demanding and expensive requirements greatly limited large-scale fabrication and application. Therefore, exploiting fabrication approaches with simple, fast, low-energy consumption, and possibility on a large-area preparation are still of great significance.

II. Introducing low-surface energy substances is one of the crucial factors for constructing superhydrophobic surface. In order to achieve or recover the superhydrophobicity, perfluoro-compounds were frequently applied in the existing methods. However, these fluorine-containing substances usually possess high prices and low stability. The degraded or released components also showed side effects on human beings, wildlife, and environments. Such safety issues also greatly limited the application of the surfaces. Thus, it is crucial for the researchers to develop nontoxic and fluorine-free substances with low-surface energy to replace the fluorine-containing materials.

III. Even though various self-healing superhydrophobic surfaces with enhanced durability have been developed, this excellent durability of certain surfaces often relies on the texture of substrates, for example, textiles, which highly restrict the application areas. Robust superhydrophobic surfaces fabricated on different kinds of substrates, especially smooth substrates, still need to be developed to repair damage on a larger scale. To overcome this issue, computational intelligence will be a useful method to predict and optimize the properties of superhydrophobic surfaces in a fast and efficient manner.[59]

IV. The speed of self-healing behavior is another critical factor for the application of superhydrophobic surfaces. The long healing process (hours or even days) makes the surface unsuitable for practical use. Developing superhydrophobic surfaces with ultra-fast self-healing property (fully recovered in seconds or minutes) is extremely important for various outdoor applications like anti-corrosion.

V. The initiation of the self-healing process should be optimized. As reported in previous work, most of the self-healing processes were triggered by external stimuli, for example, humidity, heat, pH, light, etc. It is still a great challenge to achieve the appropriate stimuli to initiate the healing process in diverse practical applications. Therefore, designing self-healing superhydrophobic surfaces, whose surface wettability could be restored under practical conditions or even without external treatments, is highly desirable.

We hope that the overviewed recovery principles and applications of self-healing superhydrophobic surfaces can help readers quickly catch the recent progress of this kind of functional

Table 1. Summary of self-healing superhydrophobic surfaces with specific materials, healing process, and applications.

Materials	Self-healing agents/processes	Trigger	Applications	Ref.
PDMS, *n*-nonadecane	*n*-nonadecane	AT		[13]
PAH-PEEK, PAA, PFOS/POTS	PFOS/POTS	40% RH		[14,15c]
bPEI, APP, FD-POSS	FD-POSS	35% RH	Fame-retardant coating	[15a]
POS latex, FMS, TiO_2 NPs, FAS13	FAS-13	UV	Self-cleaning	[15b]
Porous alumina, FDPA, PFDS	PFDS	AT		[15d]
Al_2O_3 NPs, POTS, aluminum nitrate	POTS	100 °C	Self-cleaning, waterproof	[15e]
PTFE NPs, cationic fluorosurfactant (DuPont Zonyl321), PFDS	PFDS	135 °C		[15f]
cellulose-silica microcapsules, *n*-octadecane	*n*-octadecane	80 °C	Ultraviolet resistance, thermal insulation	[16]
FAS-12 loaded microcapsules, FAS-17-modified SiO_2 NPs, polysiloxane latex,	FAS-12	UV		[17]
POS/MWCNTs nanocomposites	POS	Toluene/240 °C		[18a]
Rough aluminum, PDMS	Cyclic oligomers generated from PDMS decomposition	350 °C		[18b]
PUF microcapsules, HDI	HDI	AT	Anticorrosion, antifouling	[18c]
PDA nanocapsules, ODA	ODA	80 °C	Self-cleaning	[18d]
H_3BO_3-incorporated SiO_2-alkyl-silane, PDMS	PDMS	AT	Self-cleaning, oil–water separation	[19]
ODA@PDA core-shell nanospheres	ODA	Sunlight	Superhydrophobic fabrics	[20]
Aluminum phosphate, TiO_2 NPs, OTS	OTS	200 °C	Oil–water separation	[22]
ZrP nanoplates, ODA	ODA	AT/60 °C	Oil–water separation	[23]
CF7	CF7	Microwave	AT	[24b]
Aluminum	Organic materials formed during laser ablation	AT	Anti-corrosion	[41]
TiO_2 NPs, PDMS	PDMS	AT	Oil–water separation	[45]
SiO_2 NPs, silicon rubber	Silicon rubber	AT	Oil–water separation	[46]
PU, SiO_2@HD-POS	HD-POS	150 °C	Anti-icing	[52]
PVDF NPs, PI film, PFDS	PFDS	60 °C	Water-energy harvesting	[54]
Beeswax, MWCNTs, PDMS	Bee wax	70 °C	Solar steam generation	[55]
Ni_3S_2, myristic acid	Myristic acid	AT	(Anti)-condensation	[56a]
F-PVDF/Fe_3O_4@PPyx, PFDS	PFDS	50% RH	Superior microwave absorption	[57]
3M Super 77 Multipurpose Spray Adhesive, H-SiO2 NPs	Surface structure re-arrangement	Acetone	Building materials	[24c]
bPEI, PVDMA, n-decylamine	Surface topology regeneration	Water		[24d]
KH570 grafted nano-SiO_2, ACNTB, EP	Physical structure regeneration	300 °C	Self-cleaning, anti-fouling	[25]
ZNO, PMMA, STA	Regeneration of the topographic structures	Water		[26]
PDMS, PFMA	Regeneration of the topographic structures	DMF	Drag reduction	[28]
PCL, PVA, AgNPs-AgNWs, PFDT	Bulk material healing driven the recovery of topographic structures	Voltage/near-infrared light		[29]
$FeCl_3$, AB, GA-PDMS, TiO_2 NPs, super P, PFDS	Bulk material healing driven the arrangements of nanoparticles	DC power	Anti-icing	[30]
Epoxidized soybean oil, perfluorinated EP, citric acid, SiO_2 NPs	Bulk material healing driven the recovery of topographic structures	60 °C	Anti-corrosion	[43]
DGEBA, n-octylamine, MXDA	SMP	120 °C	Droplet manipulation	[31b,32]
BADGE, Jeffamine D230, n-decylamine, BTA, epoxy based SMP	SMP	60 °C	Anti-corrosion	[31c]
Epoxy-based SMP	SMP	80–120 °C	Droplet storage	[33–34]
EP resins and PDMS	Shape memory effect of epoxy resin	85–125 °C		[35]
bPEI, AGO, 5Acl, n-decylamine	Absolutely self-healable material	AT	Droplet manipulation	[37]

Table 1. Continued.

Materials	Self-healing agents/processes	Trigger	Applications	Ref.
EP resin, PF-POS@silica	Shape memory effect of epoxy resin	60–80 °C	Corrosion protection of Mg alloy	[42]
Resin matrix, fluorinated SiO_2 NPs	Shape memory effect of epoxy resin	100 °C	Drag reduction	[50]
Alginate-based aerogel, Ag NPs, ODA	Dynamic catechol–Fe coordination, transportation of ODA	70 °C		[38a]
Polystyrene, FMS, TiO_2 NPs, PMSF	SiO_2 and TiO_2 NPs re-arrangenment, transportation of PMSF	UV	Self-cleaning	[38b]
BiOCl, FAS-13	Re-arrangement of BiOCl, transportation of FAS-13	150 °C	Degradation of organic dyes	[38c]
Al_2O_3 NPs, PHME, ODPA, HDDA	Self-organization of particles, transportation of ODPA	100 °C		[38d]
FMS, FAS, FD-POSS	Re-arrangement of FD-POSS and SiO_2 nanoparticles, transportation of FAS	140 °C		[39]
Epoxy-based SMP, DGEBA, *n*-octylamine, MXDA	Shape memory effect of epoxy resin and transportation of polymer chains	85 °C		[40]
PU-C_8F_{17}	PU-C_8F_{17}	50 °C	Oil–water separation	[47]

Additional abbreviations: ambient temperature (AT), ammonium polyphosphate (APP), α, ω-bis(hydroxypropyl)-terminated poly(2,2,3,3,4,4,4-heptafluoro-butylmethylsiloxane) (PMSF), bisphenol A diglycidyl ether (BADGE), branched poly(ethylenimine) (bPEI), diglycidyl ether of bisphenol A type epoxy resin (DGEBA), dipentaerythritol penta-acrylate (5Acl), fluorinated SiO_2 nanoparticles (FMS), hexamethylene diisocyanate (HDI), 1,6-hexanediol diacrylate (HDDA), hydrophobic SiO_2 nanoparticles (H-SiO_2 NPs), multiwalled carbon nanotubes (MWCNTs), nanoparticles (NPs), (±)-N,N′-(trans-cyclohexane-1,2-diyl) bis (2,2,3,3,4,4,5,5,6,6,7,7,8,8,8-penta-decafluorooctan-amide) (CF7), octadecylphosphonic acid (ODPA), 1H,1H,2H,2H-perfluorodecylphosphonic acid (FDPA), phosphoric acid 2-hydroxyethyl methacrylate ester (PHME), polypyrrole (PPyx), polysiloxane (POS), poly(urea-formaldehyde) (PUF), poly(vinyl-4,4-dimethylazlac-tone) (PVDMA), polyvinylidene fluorid (PVDF), *m*-Xylylenediamine (MXDA).

surfaces. We believe that a bright future of self-healing superhydrophobic surfaces will be witnessed. More simple and powerful strategies of fabricating self-healing superhydrophobic surfaces will be developed from fundamental research and practical applications soon by the efforts of researchers.

Acknowledgements

W.L. acknowledges the Max Planck Center for Complex Fluid Dynamics and the ERC advanced grant 340391 SUPRO for financial support.

Open access funding enabled and organized by Projekt DEAL.

Conflict of Interest

The authors declare no conflict of interest.

Keywords

anti-corrosion, drag reduction, liquid transportation, oil/water separation, regeneration of hierarchical topography, self-healing, superhydrophobic surfaces

Received: February 16, 2021
Revised: March 22, 2021
Published online: May 24, 2021

[1] a) M. Ma, R. M. Hill, *Curr. Opin. Colloid Interface Sci.* **2006**, *11*, 193; b) E. Kobina Sam, D. Kobina Sam, X. Lv, B. Liu, X. Xiao, S. Gong, W. Yu, J. Chen, J. Liu, *Chem. Eng. J.* **2019**, *373*, 531; c) S. Wang, K. Liu, X. Yao, L. Jiang, *Chem. Rev.* **2015**, *115*, 8230; d) W. Liu, S. Xiang, X. Liu, B. Yang, *ACS Nano* **2020**, *14*, 9166; e) S. Zhou, L. Jiang, Z. Dong, *Adv. Mater. Interfaces* **2021**, *8*, 2000824.

[2] a) T. Darmanin, F. Guittard, *Mater. Today* **2015**, *18*, 273; b) S. Parvate, P. Dixit, S. Chattopadhyay, *J. Phys. Chem. B* **2020**, *124*, 1323; c) X.-M. Li, D. Reinhoudt, M. Crego-Calama, *Chem. Soc. Rev.* **2007**, *36*, 1350; d) W. Liu, X. Liu, S. Xiang, Y. Chen, L. Fang, B. Yang, *Nano Res.* **2016**, *9*, 3141.

[3] a) F. Zhang, L. Zhao, H. Chen, S. Xu, D. G. Evans, X. Duan, *Angew. Chem., Int. Ed.* **2008**, *47*, 2466; b) Z. Guo, F. Zhou, J. Hao, W. Liu, *J. Am. Chem. Soc.* **2005**, *127*, 15670.

[4] R. Blossey, *Nat. Mater.* **2003**, *2*, 301.

[5] J. Genzer, K. Efimenko, *Biofouling* **2006**, *22*, 339.

[6] a) M. Guix, J. Orozco, M. García, W. Gao, S. Sattayasamitsathit, A. Merkoçi, A. Escarpa, J. Wang, *ACS Nano* **2012**, *6*, 4445; b) L. Feng, Z. Zhang, Z. Mai, Y. Ma, B. Liu, L. Jiang, D. Zhu, *Angew. Chem., Int. Ed.* **2004**, *43*, 2012.

[7] a) K. Koch, B. Bhushan, Y. C. Jung, W. Barthlott, *Soft Matter* **2009**, *5*, 1386; b) C.-H. Xue, J.-Z. Ma, *J. Mater. Chem. A* **2013**, *1*, 4146; c) C. Cottin-Bizonne, J.-L. Barrat, L. Bocquet, E. Charlaix, *Nat. Mater.* **2003**, *2*, 237; d) X. Gao, X. Yan, X. Yao, L. Xu, K. Zhang, J. Zhang, B. Yang, L. Jiang, *Adv. Mater.* **2007**, *19*, 2213; e) M. Ferrari, A. Benedetti, *Adv. Colloid Interface Sci.* **2015**, *222*, 291; f) W. Liu, J. Midya, M. Kappl, H.-J. Butt, A. Nikoubashman, *ACS Nano* **2019**, *13*, 4972; g) W. Liu, M. Kappl, H.-J. Butt, *ACS Nano* **2019**, *13*, 13949; h) W. Liu, X. Liu, J. Fangteng, S. Wang, L. Fang, H. Shen, S. Xiang, H. Sun, B. Yang, *Nanoscale* **2014**, *6*, 13845.

[8] a) K. Ellinas, A. Tserepi, E. Gogolides, *Adv. Colloid Interface Sci.* **2017**, *250*, 132; b) K. Chen, Y. Wu, S. Zhou, L. Wu, *Macromol. Rapid Commun.* **2016**, *37*, 463.

[9] T. Verho, C. Bower, P. Andrew, S. Franssila, O. Ikkala, R. H. A. Ras, *Adv. Mater.* **2011**, *23*, 673.

[10] a) S. Gao, X. Dong, J. Huang, J. Dong, Y. Cheng, Z. Chen, Y. Lai, *Appl. Surf. Sci.* **2018**, *459*, 512; b) Y.-Y. Quan, Z. Chen, Y. Lai, Z.-S. Huang, H. Li, *Mater. Chem. Front.* **2021**, *5*, 1655.

[11] L. Ionov, A. Synytska, *Phys. Chem. Chem. Phys.* **2012**, *14*, 10497.

[12] C. Zhang, F. Liang, W. Zhang, H. Liu, M. Ge, Y. Zhang, J. Dai, H. Wang, G. Xing, Y. Lai, Y. Tang, *ACS Omega* **2020**, *5*, 986.

[13] Y. Wang, Y. Liu, J. Li, L. Chen, S. Huang, X. Tian, *Chem. Eng. J.* **2020**, *390*, 124311.
[14] Y. Li, S. Chen, M. Wu, J. Sun, *Adv. Mater.* **2014**, *26*, 3344.
[15] a) S. Chen, X. Li, Y. Li, J. Sun, *ACS Nano* **2015**, *9*, 4070; b) Q. Rao, K. Chen, C. Wang, *RSC Adv.* **2016**, *6*, 53949; c) Y. Li, L. Li, J. Sun, *Angew. Chem., Int. Ed.* **2010**, *49*, 6129; d) K. Nakayama, A. Koyama, C. Zhu, Y. Aoki, H. Habazaki, *Adv. Mater. Interfaces* **2018**, *5*, 1800566; e) Y. Lee, E.-A. You, Y.-G. Ha, *Appl. Surf. Sci.* **2018**, *445*, 368; f) H. Zhou, H. Wang, H. Niu, Y. Zhao, Z. Xu, T. Lin, *Adv. Funct. Mater.* **2017**, *27*, 1604261.
[16] K. Chen, J. Zhou, X. Che, R. Zhao, Q. Gao, *J. Colloid Interface Sci.* **2020**, *566*, 401.
[17] K. Chen, S. Zhou, S. Yang, L. Wu, *Adv. Funct. Mater.* **2015**, *25*, 1035.
[18] a) B. Li, J. Zhang, *Carbon* **2015**, *93*, 648; b) M. Long, S. Peng, W. Deng, X. Yang, K. Miao, N. Wen, X. Miao, W. Deng, *J. Colloid Interface Sci.* **2017**, *508*, 18; c) G. Wu, J. An, X.-Z. Tang, Y. Xiang, J. Yang, *Adv. Funct. Mater.* **2014**, *24*, 6751; d) Y. Liu, Z. Liu, Y. Liu, H. Hu, Y. Li, P. Yan, B. Yu, F. Zhou, *Small* **2015**, *11*, 426.
[19] S. K. Lahiri, P. Zhang, C. Zhang, L. Liu, *ACS Appl. Mater. Interfaces* **2019**, *11*, 10262.
[20] J. Zhang, J. Zhao, W. Qu, Z. Wang, *Mater. Chem. Front.* **2019**, *3*, 1341.
[21] a) H. Lee, S. M. Dellatore, W. M. Miller, P. B. Messersmith, *Science* **2007**, *318*, 426; b) Y. Liu, K. Ai, L. Lu, *Chem. Rev.* **2014**, *114*, 5057; c) Z. Wang, S. Ji, J. Zhang, Q. Liu, F. He, S. Peng, Y. Li, *J. Mater. Chem. A* **2018**, *6*, 13959.
[22] M. Liu, Y. Hou, J. Li, L. Tie, Y. Peng, Z. Guo, *J. Mater. Chem. A* **2017**, *5*, 19297.
[23] M. Zeng, P. Wang, J. Luo, B. Peng, B. Ding, L. Zhang, L. Wang, D. Huang, I. Echols, E. Abo Deeb, E. Bordovsky, C.-H. Choi, C. Ybanez, P. Meras, E. Situ, M. S. Mannan, Z. Cheng, *ACS Appl. Mater. Interfaces* **2018**, *10*, 22793.
[24] a) G. Xi, J. Wang, G. Luo, Y. Zhu, W. Fan, M. Huang, H. Wang, X. Liu, *Cellulose* **2016**, *23*, 915; b) Q. Wei, C. Schlaich, S. Prévost, A. Schulz, C. Böttcher, M. Gradzielski, Z. Qi, R. Haag, C. A. Schalley, *Adv. Mater.* **2014**, *26*, 7358; c) U. Zulfiqar, M. Awais, S. Z. Hussain, I. Hussain, S. W. Husain, T. Subhani, *Mater. Lett.* **2017**, *192*, 56; d) U. Manna, D. M. Lynn, *Adv. Mater.* **2013**, *25*, 5104; e) B. Li, L. Kan, S. Zhang, Z. Liu, C. Li, W. Li, X. Zhang, H. Wei, N. Ma, *Nanoscale* **2019**, *11*, 467.
[25] Z. Wang, L. Yuan, G. Liang, A. Gu, *Chem. Eng. J.* **2021**, *408*, 127263.
[26] N. Bai, Q. Li, H. Dong, C. Tan, P. Cai, L. Xu, *Chem. Eng. J.* **2016**, *293*, 75.
[27] a) K. Tanaka, Y. Fujii, H. Atarashi, K.-i. Akabori, M. Hino, T. Nagamura, *Langmuir* **2008**, *24*, 296; b) B. Jing, J. Zhao, Y. Wang, X. Yi, H. Duan, *Langmuir* **2010**, *26*, 7651; c) M. N'Diaye, F. Pascaretti-Grizon, P. Massin, M. F. Baslé, D. Chappard, *Langmuir* **2012**, *28*, 11609.
[28] Y. Liu, H. Gu, Y. Jia, J. Liu, H. Zhang, R. Wang, B. Zhang, H. Zhang, Q. Zhang, *Chem. Eng. J.* **2019**, *356*, 318.
[29] M. Wu, Y. Li, N. An, J. Sun, *Adv. Funct. Mater.* **2016**, *26*, 6777.
[30] L. Qin, Y. Chu, X. Zhou, Q. Pan, *ACS Appl. Mater. Interfaces* **2019**, *11*, 29388.
[31] a) D. Zhang, Z. Cheng, Y. Liu, *Chem. - Eur. J.* **2019**, *25*, 3979; b) Z. Cheng, D. Zhang, T. Lv, H. Lai, E. Zhang, H. Kang, Y. Wang, P. Liu, Y. Liu, Y. Du, S. Dou, L. Jiang, *Adv. Funct. Mater.* **2018**, *28*, 1705002; c) H. Qian, D. Xu, C. Du, D. Zhang, X. Li, L. Huang, L. Deng, Y. Tu, J. M. C. Mol, H. A. Terryn, *J. Mater. Chem. A* **2017**, *5*, 2355.
[32] H. Zhang, H. Lai, Z. Cheng, D. Zhang, P. Liu, Y. Li, Y. Liu, *Appl. Surf. Sci.* **2020**, *525*, 146525.
[33] C.-M. Chen, S. Yang, *Adv. Mater.* **2014**, *26*, 1283.
[34] T. Lv, Z. Cheng, D. Zhang, E. Zhang, Q. Zhao, Y. Liu, L. Jiang, *ACS Nano* **2016**, *10*, 9379.
[35] X.-J. Guo, C.-H. Xue, S. Sathasivam, K. Page, G. He, J. Guo, P. Promdet, F. L. Heale, C. J. Carmalt, I. P. Parkin, *J. Mater. Chem. A* **2019**, *7*, 17604.
[36] W. Wang, J. Salazar, H. Vahabi, A. Joshi-Imre, W. E. Voit, A. K. Kota, *Adv. Mater.* **2017**, *29*, 1700295.
[37] A. Das, J. Deka, K. Raidongia, U. Manna, *Chem. Mater.* **2017**, *29*, 8720.
[38] a) L. Qin, N. Chen, X. Zhou, Q. Pan, *J. Mater. Chem. A* **2018**, *6*, 4424; b) K. Chen, S. Zhou, L. Wu, *Chem. Commun.* **2014**, *50*, 11891; c) S. Jia, Y. Lu, S. Luo, Y. Qing, Y. Wu, I. P. Parkin, *Chem. Eng. J.* **2019**, *366*, 439; d) Y. Lee, E.-A. You, Y.-G. Ha, *ACS Appl. Mater. Interfaces* **2018**, *10*, 9823.
[39] H. Wang, H. Zhou, A. Gestos, J. Fang, T. Lin, *ACS Appl. Mater. Interfaces* **2013**, *5*, 10221.
[40] T. Lv, Z. Cheng, E. Zhang, H. Kang, Y. Liu, L. Jiang, *Small* **2017**, *13*, 1503402.
[41] G. Yuan, Y. Liu, C.-V. Ngo, C. Guo, *Opt. Express* **2020**, *28*, 35636.
[42] X. Zhao, J. Wei, B. Li, S. Li, N. Tian, L. Jing, J. Zhang, *J. Colloid Interface Sci.* **2020**, *575*, 140.
[43] M. Ezazi, B. Shrestha, N. Klein, D. H. Lee, S. Seo, G. Kwon, *ACS Appl. Mater. Interfaces* **2019**, *11*, 30240.
[44] C. Ding, Y. Liu, M. Wang, T. Wang, J. Fu, *J. Mater. Chem. A* **2016**, *4*, 8041.
[45] H. Zhu, L. Wu, X. Meng, Y. Wang, Y. Huang, M. Lin, F. Xia, *Nanoscale* **2020**, *12*, 11455.
[46] L. Liu, Y. Shan, M. Pu, X. Zhao, Y. Huang, *Macromol. Chem. Phys.* **2020**, *221*, 1900356.
[47] W. Fang, L. Liu, T. Li, Z. Dang, C. Qiao, J. Xu, Y. Wang, *Chem. - Eur. J.* **2016**, *22*, 878.
[48] a) T. Lee, E. Charrault, C. Neto, *Adv. Colloid Interface Sci.* **2014**, *210*, 21; b) E. Lauga, H. A. Stone, *J. Fluid Mech.* **2003**, *489*, 55; c) A. M. J. Davis, E. Lauga, *J. Fluid Mech.* **2010**, *661*, 402; d) E. S. Asmolov, S. Schmieschek, J. Harting, O. I. Vinogradova, *Phys. Rev. E* **2013**, *87*, 023005; e) J. P. Rothstein, *Annu. Rev. Fluid Mech.* **2009**, *42*, 89.
[49] D. Schäffel, K. Koynov, D. Vollmer, H.-J. Butt, C. Schönecker, *Phys. Rev. Lett.* **2016**, *116*, 134501.
[50] Y. Liu, J. Liu, Y. Tian, H. Zhang, R. Wang, B. Zhang, H. Zhang, Q. Zhang, *Ind. Eng. Chem. Res.* **2019**, *58*, 4468.
[51] K. M. T. Ahmmed, J. Montagut, A.-M. Kietzig, *Can. J. Chem. Eng.* **2017**, *95*, 1934.
[52] Y. Li, B. Li, X. Zhao, N. Tian, J. Zhang, *ACS Appl. Mater. Interfaces* **2018**, *10*, 39391.
[53] a) K. Chen, K. Gu, S. Qiang, C. Wang, *RSC Adv.* **2017**, *7*, 543; b) Y. Wang, J. Xue, Q. Wang, Q. Chen, J. Ding, *ACS Appl. Mater. Interfaces* **2013**, *5*, 3370.
[54] Y. Liu, Y. Zheng, T. Li, D. Wang, F. Zhou, *Nano Energy* **2019**, *61*, 454.
[55] D. Weng, F. Xu, X. Li, Y. Li, J. Sun, *J. Mater. Chem. A* **2018**, *6*, 24441.
[56] a) X. Yin, S. Yu, Y. Zhao, E. Liu, K. Wang, *J. Taiwan Inst. Chem. Eng.* **2019**, *99*, 268; b) X. Yan, Z. Huang, S. Sett, J. Oh, H. Cha, L. Li, L. Feng, Y. Wu, C. Zhao, D. Orejon, F. Chen, N. Miljkovic, *ACS Nano* **2019**, *13*, 4160.
[57] Y. Li, Y. Zhao, X. Lu, Y. Zhu, L. Jiang, *Nano Res.* **2016**, *9*, 2034.
[58] a) K. Tu, X. Wang, L. Kong, H. Guan, *Mater. Des.* **2018**, *140*, 30; b) Y. Shen, Y. Wu, Z. Shen, H. Chen, *Coatings* **2018**, *8*, 144.
[59] a) A. Azimi Yancheshme, S. Hassantabar, K. Maghsoudi, S. Keshavarzi, R. Jafari, G. Momen, *Chem. Eng. J.* **2020**, 127898; b) X. Zhang, B. Ding, R. Cheng, S. C. Dixon, Y. Lu, *Adv. Sci.* **2018**, *5*, 1700520; c) S. Subianto, C. Li, D. Rubin de Celis Leal, S. Rana, S. Gupta, R. He, S. Venkatesh, A. Sutti, *ACS Omega* **2019**, *4*, 15912.

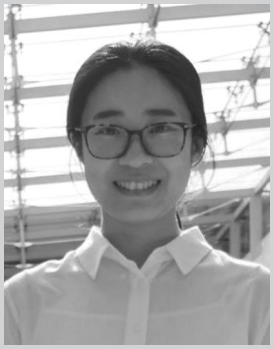

Siyuan Xiang studied polymer chemistry and physics at Jilin University, and defended her Ph.D. thesis in 2017 under the supervision of Prof. Bai Yang at the State Key Laboratory of Supramolecular Structure and Materials (SKLSSM). Then she went to Mainz and joined the group of Prof. Tanja Weil at the Max Planck Institute for Polymer Research (MPIP) as a postdoc. Her research interests focus on functional surfaces/interfaces and materials, supramolecular interaction for biomedical applications.

Wendong Liu is an associate professor at Dalian University of Technology (DUT), Dalian China. He studied polymer chemistry and physics at Jilin University, and defended his Ph.D. thesis in 2017 under the supervision of Prof. Bai Yang at the State Key Laboratory of Supramolecular Structure and Materials. Then he joined the Physics at Interfaces group of Prof. Hans-Jürgen Butt at the Max Planck Institute for Polymer Research (MPIP) as a postdoc. In 2021, he became an associate professor at DUT. His research interests focus on supraparticles, super liquid repellent surfaces, and functional surfaces/interfaces mediated controllable adhesion.